Stochastic in Space and Time: Part 1, Characterizing Orographic Gradients in Mean Runoff and Daily Runoff Variability

A.M. Forte[1] and M.W. Rossi[2]

[1] Department of Geology and Geophysics, Louisiana State University, Baton Rouge, Louisiana, USA.
[2] Earth Lab, Cooperative Institute for Research in Environmental Sciences (CIRES), University of Colorado, Boulder, Colorado, USA.

Corresponding author: Adam M. Forte (aforte8@lsu.edu)

Key Points:

- WaterGAP3 water model data overestimates daily runoff variability in snowmelt influenced watersheds
- Global relationships between mean runoff and daily runoff variability is strongly mediated by snowmelt fraction
- Topographic drivers of mean runoff, snowmelt fraction, and daily runoff variability are best assessed at the mountain range scale

Abstract

Mountain topography alters the phase, amount, and spatial distribution of precipitation. Past efforts focused on how orographic precipitation alters runoff spatial distribution, but with less emphasis on how stochastic runoff generation is also patterned on topography. Given the importance of the magnitude and frequency of stochastic runoff events to fluvial erosion, we evaluate whether orographic patterns in mean runoff and daily runoff variability can be constrained using the global WaterGAP3 water model data. Model runoff data is validated against observational data in the contiguous United States, showing agreement with mean runoff in all settings and daily runoff variability in settings where rainfall-runoff predominates. In snowmelt-influenced settings, runoff variability is overestimated by the water model data. Cognizant of these limitations, we use the water model data to develop relationships between mean runoff and daily runoff variability and how these are mediated by snowmelt fraction in mountain topography globally. Attempts to explain topographic controls on hydro-climatic variables using a Random Forest Regression model were less clear. Instead, relationships between topography and runoff parameters are better assessed at mountain range scale. Rulesets linking topography to mean runoff and snowmelt fraction are developed for three mid-latitude mountain landscapes—British Columbia, European Alps, and Greater Caucasus. Increasing topographic elevation and relief together lead to higher mean runoff and lower runoff variability due to the increasing contribution of snowmelt. The three sets of empirical relationships developed here serve as the basis for a suite of numerical experiments in our companion manuscript to this one (Part 2).

Plain Language Summary

It has long been understood that mountain ranges can have profound influences on the location and intensity of precipitation, for example through the formation of rain shadows. Less clear is how these "orographic effects" are reflected in the details of streamflow, specifically the variability of streamflow. Understanding variability of streamflow, or runoff, is important as differences in variability directly influence the erosional form of river long profiles, and thus the relief of landscapes. Here we use results from a global water model integrated with topography data to explore how runoff variability is related to topography in high relief landscapes. Consistent with prior work, we find and expand on the observation that mean runoff and runoff variability are inversely correlated and that the nature of their relation fundamentally depends on the importance of snowmelt. In turn, both mean runoff and the importance of snowmelt are positively correlated with aspects of topography. Our results imply that incorporating variability into models of coupled orography and landscape evolution is critical and we identify a simple framework within which to develop such models. Examples of these models are presented in a companion work (Part 2).

1 Introduction

Weather systems develop over the course of hours to weeks depending on their size (e.g., Trenberth et al., 2003), while landscapes evolve over millennia and longer. How climate drives the long-term evolution of mountain belts (Whipple, 2009) is impeded by this mismatch in timescale. Modeling weather and hydrology over long timescales is a substantial computational challenge (e.g., Shen et al., 2021), and thus the choices made in representation of the hydro-

climate are often baked into the simplified process laws we use to construct landscape evolution models. For fluvial landscapes, the most widely used model for river incision and relief development is the stream power model (Howard, 1994; Whipple & Tucker, 1999). The shear stress formulation of stream power asserts that fluvial erosion can be expressed as the product of three terms: a coefficient describing the efficiency of erosion, drainage area raised to an exponent, and local slope raised to another exponent. The latter two terms and the ratio of the exponents can be constrained using topographic data alone (e.g., Wobus et al., 2006), leaving the coefficient of erosion to account for a large number of important process parameters including climate. While unpacking the assumptions underlying generalized forms of stream power have been addressed by many papers (e.g., Kirby & Whipple, 2012; Lague, 2014; Whipple et al., 2022), we highlight two sets of assumptions of stream power that motivate our analysis of global runoff data. First, it is common to use drainage area as a proxy for discharge. Orographic precipitation (Galewsky, 2009; Roe, 2005) is mimicked in 1D stream power models by adding an additional area dependence on runoff that alters concavity (Roe et al., 2002) and fluvial relief (Roe et al., 2003). In 2D, these basic effects tend to be more ambiguous (Han et al., 2014) and produce discordance between mainstem and tributary morphology (Leonard & Whipple, 2021). Second, stream power models typically assume a characteristic discharge, thus also assuming that erosional thresholds can be subsumed within stream power parameters. The latter assertion is not valid if erosion thresholds are important (Huang & Niemann, 2006). To address this, stochastic runoff can be accounted for in stream power by changing the temporal scale over which river erosion is modeled (i.e., at the event scale). By integrating stream power over the probability distribution of flows above erosional thresholds (Lague et al., 2005; Snyder et al., 2003; Tucker, 2004; Tucker & Bras, 2000), the response of river profiles to climate is not only embedded in the coefficient of erosion but also the effective slope exponent (DiBiase & Whipple, 2011; Lague, 2014). While the roles of both orographic precipitation and stochastic climate on stream power have each generated a lot of study on their own, there has been less effort examining them together.

Integrating orographic effects with stochastic runoff into stream power models requires better constraints on how mean runoff and runoff variability are related (or unrelated) to each other via topography. Prior studies show that mean runoff and the shape of daily runoff distributions are correlated with each other in rainfall-dominated systems (Molnar et al., 2006; Rossi et al., 2016). Figure 1B illustrates this for contiguous United States using streamflow data from the Geospatial Attributes of Gages for Evaluating Streamflow (GAGES-II) dataset (Figure 1A). Calculation of the shape parameters of each distribution are described in detail below, but we note here that high shape parameters indicate lower runoff variability. The empirical data split into two broad relationships. Separation of the two trends appears to correspond to mean annual temperatures of around 0-10° C (Figure 1B), which we hypothesize is due to relatively small changes in the fraction of mean annual streamflow that is derived from snowmelt. While prior work has examined how orographic patterns in the spatial distribution of snow alters stream power predictions (Anders et al., 2008), we are not aware of any studies showing how snowmelt alters stochastic runoff and stream power predictions. As such, coupled models of climate and tectonics using stream power (e.g., Beaumont et al., 1992; Willett, 1999) may be missing important feedbacks between topographic relief and snowmelt as mountain ranges grow.

The lack of focus on integrating orographic precipitation and stochastic runoff into stream power models is likely due to data limitations and the dearth of simple hydrological relations that can be upscaled to landscape evolution timescales. Precipitation observations

provide a starting point, though simplifying water inputs into streamflow outputs are riddled with nonlinearities that can be hard to generalize. Rainfall runoff is nonlinear due to scaling properties within watersheds and dynamical nonlinearities in hillslope runoff generation (e.g., Sivapalan et al., 2002). Furthermore, the relative contribution of different runoff generation mechanisms (i.e., extreme precipitation, soil moisture excess, snowmelt) to flood frequency is only beginning to be characterized under modern climate conditions (e.g., Berghuijs et al., 2019), let alone for time-varying ones. Process-based hydrological models help unpack these nonlinearities for a given setting (Fatichi et al., 2016), but are typically applied at small spatial scales. Our approach is to use a global water model (Alcamo et al., 2003; Döll et al., 2003) to help constrain how topography, runoff generation, and streamflow statistics can be generalized for river incision modeling more broadly.

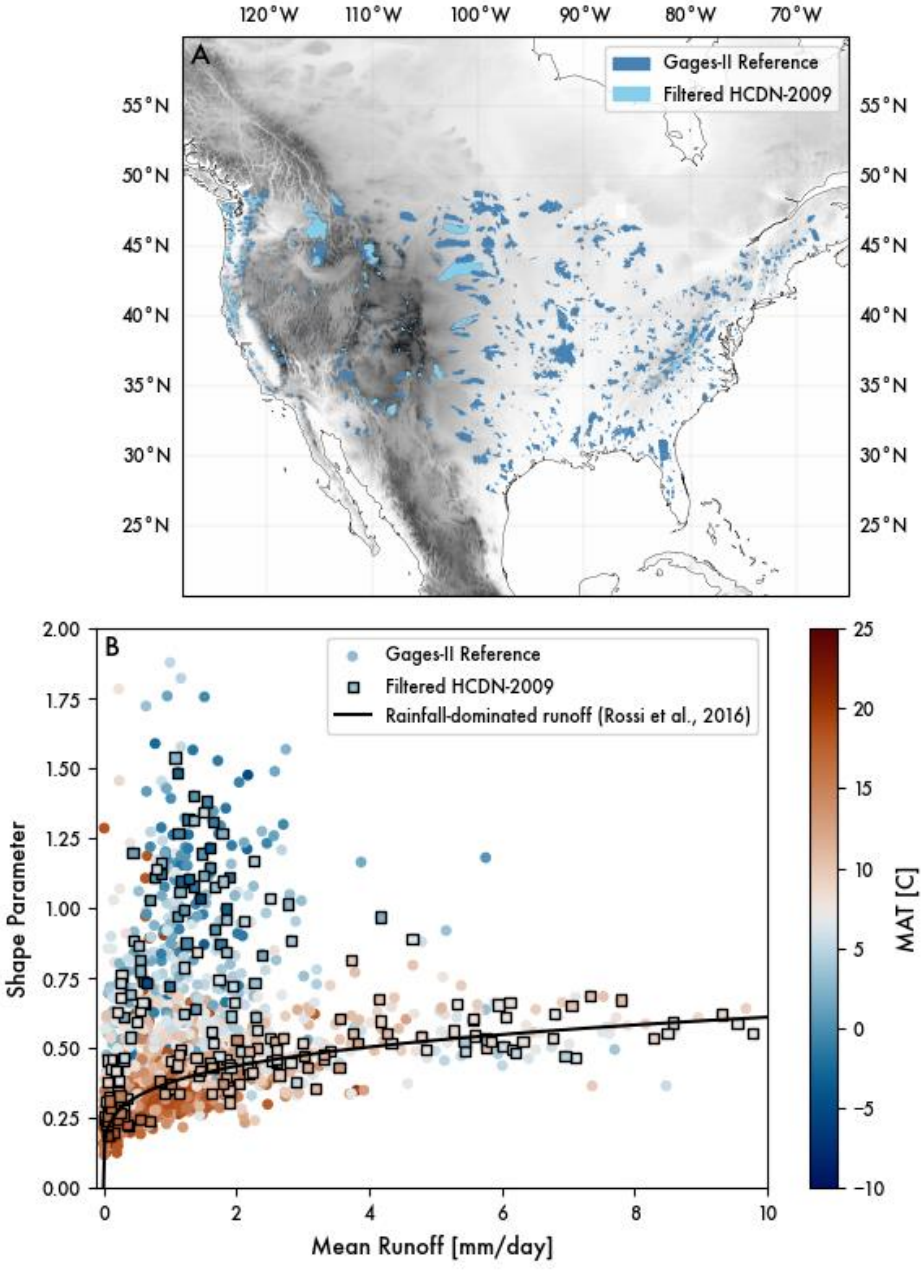

Figure 1. (A) Gauged watersheds in the contiguous United States that are minimally impacted by human management. (B) Relationship between mean runoff and the shape parameters describing daily runoff distributions for each stream gauge. In A, a subset of the reference stations in the GAGES-II network were used for the water model validation presented below (i.e., filtered HCDN-2009). In B, two broad trends between mean runoff and daily runoff variability organize around mean annual temperature, which prior authors have interpreted as reflecting the transition from snowmelt-dominated to rainfall-dominated systems (Rossi et al., 2016).

2 Background

2.1 Orographic effects

Topography perturbs the equilibrium structure of the atmosphere by adding roughness, obstructing air masses, and serving as a heat source (Smith, 1979). The conventional treatment of orographic precipitation in landscape evolution studies (e.g., Beaumont et al., 1992; Willett, 1999) focuses on the thermodynamic implications of mountain topography on how precipitation is extracted from the atmosphere via forced ascent. The saturation vapor pressure of water in air is related to its temperature via the Clausius-Clapeyron equation (see review in Roe, 2005). As air masses move up and over mountain topography, precipitation on windward slopes increases as partially saturated air cools during ascent. A 'rain shadow' subsequently develops when the relatively drier air descends and warms on leeward slopes. This first-order description is well-rooted in atmospheric physics and observations (Barros & Lettenmaier, 1994). To extend these dynamics to air parcels flowing over more complex terrain, Smith & Barstad (2004) developed a linear model of orographic precipitation that accounts for atmospheric dynamics, upwind advection, and downslope evaporation. Because settling velocities of snow are an order of magnitude slower than rain, this model can be used to examine how snow alters the spatial distribution of water inputs (Anders et al., 2008). However, one notable limitation to the linear model of orographic precipitation is that it does not account for the blocking of air by terrain, a nonlinear process that depends on the Brunt-Vaisala frequency describing the horizontal propagation of waves, horizontal windspeed, and orogen-scale relief (Barros & Lettenmaier, 1994; Galewsky, 2009; Jiang, 2003). Given that one of the key targets of landscape evolution models is to couple elevation and relief to topography through time, linear models of orographic precipitation are perhaps best suited to smaller mountain ranges.

Another approach towards characterizing orographic precipitation is to use climatological observations, especially since the advent of satellite-based remote sensing. For example, the Tropical Rainfall Measuring Mission (TRMM) was spaceborne for 17 years and provided new insights into complex spatial patterns in rainfall set up by high topography (e.g., Bookhagen & Burbank, 2006; Bookhagen & Strecker, 2008; Deal et al., 2017; Forte et al., 2016; Nesbitt & Anders, 2009). One of the key insights from these studies is the central importance of local relief to driving spatial patterns in rainfall. For example, in the Himalaya, TRMM rainfall revealed two narrow bands of rainfall that correspond to abrupt physiographic transitions into the Lesser Himalaya and into the Greater Himalaya which had not been previously identified (Bookhagen & Burbank, 2006, 2010). As such, spatial patterns derived from TRMM rainfall are increasingly being used to inform interpretations of river channel profiles (Adams et al., 2020; Bookhagen & Strecker, 2011; Leonard et al., 2023), though these approaches typically assume mean rainfall is directly proportional mean runoff. While other remote sensing products like MODIS can also

help constrain snow cover to construct a full water budget (Bookhagen & Burbank, 2010), such products tend to require temperature-index or process-based hydrological models to reliably estimate snowmelt contributions to streamflow (Walter et al., 2005).

Given the importance of snowmelt to streamflow in mid-latitude mountain ranges (Barnett et al., 2005; Barnhart et al., 2016), the difficulty of obtaining direct estimates of snowmelt leads to substantial uncertainty when using remotely sensed rainfall data as a proxy for runoff. Altering the phase of precipitation can cause up to 100% reductions in snowmelt contributions to streamflow in settings near the freezing temperature window (Adam et al., 2009). This has prompted some authors to suggest that climate change driven reductions in snowmelt fraction generally leads to lower streamflow as snowfall gives way to rain (Berghuijs et al., 2014). Such arguments rest on the premise that snowmelt runoff will lead to higher runoff ratios, all other things being equal, because solid water is stored in the snowpack and released more slowly than rainfall runoff. Better understanding of orographic effects on the snowmelt contribution to streamflow in mountain landscapes is sorely needed to improve stream power models of river incision.

2.2 Stochastic river incision

Early efforts to integrate stochastic hydrology into stream power models of river incision (Snyder et al., 2003; Tucker, 2004; Tucker & Bras, 2000) were based on the pioneering work of Eagleson (1978). By simulating rainfall events as Poisson distributions of intensities, durations, and inter-storm periods, rainfall events were represented as rectangular pulses that can be converted to runoff and routed across the landscape in order to evaluate the impact erosion thresholds on landscape evolution. Complementary efforts by Lague et al. (2005) chose to simulate streamflow directly at the daily timescale using the stochastic 'precipiton' model, which considers the time travel distribution of quanta of precipitation in order to derive streamflow distributions (Crave & Davy, 2001). By adding stochastic events to stream power, the long-term evolution of river profiles was no longer simple function of mean climate, but instead reflected a complex interplay between the frequency of large flows and erosional thresholds set by coarse sediment (Shobe et al., 2016) and the detachment of bedrock (Whipple et al., 2000). While the overall approach of these efforts was similar, the functional form of probability distributions of streamflow differed. Poisson rectangular pulses always generate light-tailed, exponential runoff distributions while the inverse gamma distribution are able to produce heavy-tailed distributions, depending on the value of shape parameter. While there is still an open question as to how heavy-tailed streamflow distributions truly are (Malamud & Turcotte, 2006; Molnar et al., 2006), the advantage of adopting these stochastic frameworks is that they are well-suited to simulating both frequent and infrequent flows and thus determining the geomorphically effective event (Huang & Niemann, 2006). Rossi et al. (2016) suggested that the stretched exponential, or Weibull, distribution might provide a flexible probability distribution that spans light-tailed to apparently heavy-tailed distributions (Laherrère & Sornette, 1998).

Regardless of how stochastic processes are represented, these early efforts prompted a large number of studies to take a closer look at whether relationships between long-term erosion rates and river morphology can be better explained using stochastic-threshold models of river incision (Campforts et al., 2020; Desormeaux et al., 2022; DiBiase & Whipple, 2011; Forte et al., 2022; Scherler et al., 2017). While success is decidedly mixed, the general outcome of using stochastic-threshold models has been to provide an alternative interpretation to nonlinear

relationships between river channel morphology and long-term erosion rates (Harel et al., 2016; Marder & Gallen, 2023). In these cases, nonlinear relationships between river morphology and long-term erosion rates arise because erosional thresholds are exceeded more frequently as erosion rate and relief increase. The climate driver on river profile evolution is not mean annual precipitation itself, but how the soil water balance (Deal et al., 2018) and the hydrologic structure of watersheds (Basso et al., 2023) mediate flood frequency. These concepts place the central focus on water storage-discharge relationships (Botter et al., 2009; Kirchner, 2009) to condition how rainfall events are converted to runoff ones. The same kind of framework can be used to account for seasonal snowmelt contributions to streamflow (Schaefli et al., 2013).

3 Datasets

Our overarching goal is to better parameterize 1D models of fluvial profile evolution that account for both stochastic events and orographic controls on runoff generation. Model development is the focus of our companion manuscript (Forte & Rossi, In Review). The focus of this manuscript is on developing empirical relationships between topography and daily runoff statistics in mountain settings that can be used to plausibly drive coupled simulations. We primarily rely on three datasets: (1) a daily, global water model derived from climate reanalysis data (WaterGAP3 data), (2) observational stream gauge data from the contiguous United States (HCDN-2009 streamflow), and (3) near global topographic data (SRTM-90 and derived HydroSHEDS v1 gridded elevation).

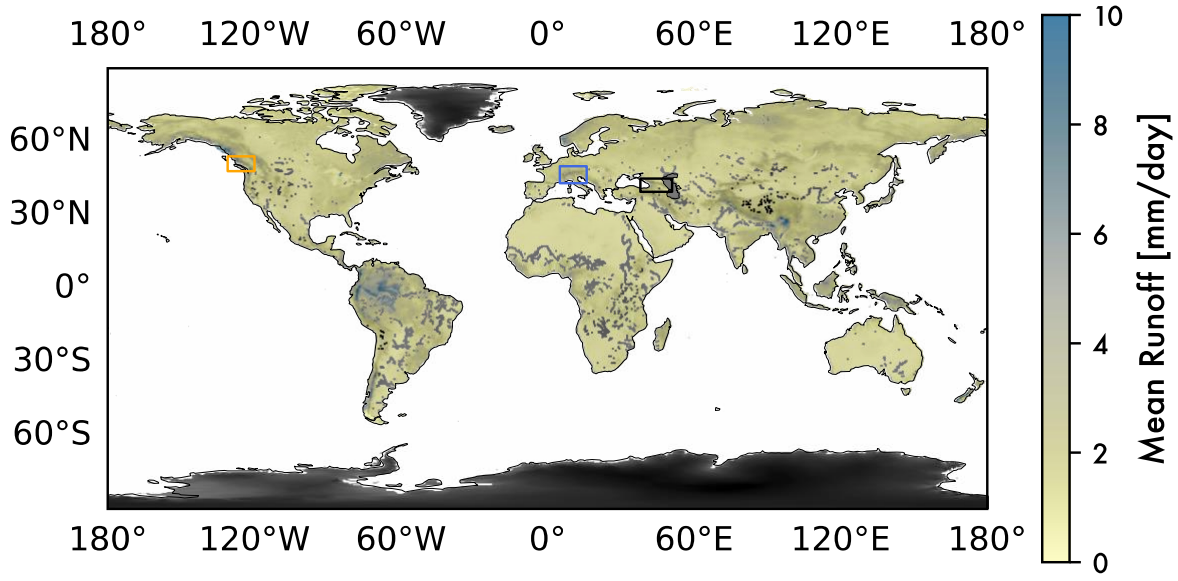

Figure 2. (A) Global mean runoff from the WaterGAP3 water model (1980-1999). The black box corresponds to the area shown in Figure 1A and bounds the geographic extent of the validation data used. The white boxes show the geographic extent of the three mid-latitude, regional case studies introduced in section 4.4.

3.1 Hydrology Data

Because streamflow data availability and quality is globally variable, we sought a single global runoff dataset that could be used to interrogate modern relationships among topography, snowmelt, and runoff. We used the Water Global Assessment and Prognosis (WaterGAP3), the most recent version of a 20+ year old global water model (Alcamo et al., 2003; Döll et al., 2003). WaterGAP3 improves on prior versions by increasing the spatial resolution from the original 0.5° to 0.25° pixel size (Eisner, 2015) and is one model included in the Earth2Observe Water Resource Reanalysis project (Schellekens et al., 2017). These model data have broad utility (e.g., Schmied et al., 2014), including for parameterization of stochastic-threshold incision models (STIM) of river incision (Campforts et al., 2020). For this analysis, we downloaded the global, 20-year, daily time series from the Earth2Observe portal (www.earth2observe.eu; last accessed April 8, 2022) spanning from January 1, 1980 to December 31, 1999.

For each pixel and day, WaterGAP3 contains a large number of input and derived hydro-climatological parameters including precipitation, runoff, discharge, and evapotranspiration. We primarily focus on the derived runoff variables from WaterGAP3, but also briefly consider temperature and precipitation. Daily average surface temperature is not distributed with WaterGAP3, so we rely on another reanalysis product of identical resolution from the Earth2Observe set, namely SURFEX-TRIP (Decharme et al., 2010, 2013). Surface temperature data is used to help interpret variation we see within the WaterGAP3 runoff data. Runoff data is subdivided into three components in WaterGAP3: surface runoff (R_s), subsurface runoff (R_{sb}), and snowmelt (R_{sm}), where total daily runoff (R_t) is the sum of the three. In the original WaterGAP3 dataset, all of these components of runoff are denoted with the variable 'Q'. We do not use this notation here given the common association of Q with discharge [L^3/t] as opposed to runoff [L/t]. For each pixel across the time-series, we calculated mean daily runoff ($\bar{R}_t$), mean daily precipitation ($\bar{P}$), means of each of the three runoff components ($\bar{R}_s$, $\bar{R}_{sb}$, $\bar{R}_{sm}$), and Weibull shape (c) and scale (R_0) parameters of the daily total runoff distributions (see section 4.1 for details). Given our interest in probing the importance of snowmelt, we also calculated the fraction of runoff contributed by snowmelt (SF), where:

$$SF = \frac{\overline{R_{sm}}}{\bar{R}_t} \quad (1)$$

Similarly, we calculate baseflow fraction of runoff (BF), where:

$$BF = \frac{\overline{R_{sb}}}{\bar{R}_t} \quad (2)$$

that we use to exclude watersheds with a substantial groundwater component to its daily fluxes.

To validate model runoff data, we used observational streamflow data from the Hydro-Climatic Data Network – 2009 (HCDN-2009) (Lins, 2012). These 743 stream gauges were identified by the USGS to be high quality, long, continuous records for watersheds with minimal impact by humans (e.g., due to landcover change, dams, and diversions). We downloaded streamflow data from the National Water Information System (NWIS) server for the dates between January 1, 1980 and December 31, 1999, to directly compare to the WaterGAP3 data. During the processing of individual HCDN-2009 time series data, any day that included

provisional or questionable data were removed and treated as NaN data. We characterize the completeness of the time series by dividing the number of days with reliable data by the total number of days. Because HCDN-2009 stream gauges are a subset of the reference stations in the Gages for Evaluating Streamflow version II (GAGES-II) network, we were able to use watershed boundaries provided by Falcone et al., (2011) to calculate watershed-averaged properties and normalize streamflow by drainage area. This latter calculation was used as an estimate for daily runoff. Processing and validation of the WaterGAP3 runoff model against HCDN-2009 observations is described in section 4.2.

3.2. Topography Data

Because we are focused on how hydroclimatic parameters vary with topography in mountain settings, it is necessary to pair the WaterGAP3 data with a global topographic dataset. We largely used the HydroSheds v1, 15-arcsecond, digital elevation model that is derived from SRTM elevation data (Lehner et al., 2008). We also used the higher resolution SRTM-90 data (Farr et al., 2007) for watershed delineation when validating WaterGAP3 against HCDN-2009 data. The HydroSheds v1 topographic data is used for two purposes: (1) To screen for portions of the global surface where orographic feedbacks with climate are relevant, and (2) To develop empirical relationships between topography and runoff statistics. With respect to data screening, we only used WaterGAP3 data where the mean elevation is greater than 250 meters above sea level and where local relief is greater than 500 meters. To calculate local relief, and avoid issues with projecting the global DEM, we calculated local relief using a circular moving window with a 2.25-minute diameter. While the exact radius in kilometers will vary as a function of latitude and more reflect an elliptical area at higher latitudes, this is approximately equal to calculating local relief with a circular moving radius of ~1-2 km at equatorial to mid-latitudes. For example, this is equivalent to an ellipse with a radius in a latitudinal direction of ~2 km, and a radius in a longitudinal direction of ~2 km (0° N/S), ~1.5 km (45° N/S), and ~1 km (60° N/S). This is a scale that prior studies have shown to linearly correlate with river channel steepness (e.g., DiBiase et al., 2010), and thus expect it to be well suited to developing empirical relationships between river morphology and local relief. The initial screening of the WaterGAP3 data using local relief is then further filtered to exclude pixels where baseflow (eq. 2) exceeds 0.25, with an eye towards minimizing the confounding factor of large groundwater contributions. To develop relationships between topography and runoff statistics we record minimum, mean, and maximum elevations within a WaterGAP3 pixel and the mean local relief within a WaterGAP3 pixel as calculated from the enclosed 60 HydroSheds pixels (i.e., there are 60 HydroShed pixels within each WaterGAP3 pixel).

4 Data Analysis

To develop empirical relationships between topography and runoff statistics from WaterGAP3, it was first important to figure out at which scale such relationships might emerge. To this end, we conduct both a global analysis and a set of regional ones that broadly correspond to the mountain range scale. These empirical relationships serve as the basis for the model development and analysis we conduct in Part 2 (Forte & Rossi, In Review). There are four main steps to the data analysis: (1) Characterization of statistical parameters for daily runoff; (2) Validation of WaterGAP3 model derived parameters with HCDN-2009 stream gage observations; (3) Global assessment of topographic controls on runoff, runoff variability, and

snowmelt fraction, and (4) Development of regionally-based relationships between topographic metrics and runoff statistics.

4.1. Daily Distributions

A number of probability distributions have been considered for the problem of bedrock river incision, including exponential (Snyder et al., 2003; Tucker, 2004), power law (Molnar et al., 2006), inverse gamma (Campforts et al., 2020; DiBiase & Whipple, 2011; Lague et al., 2005) and Weibull (Forte et al., 2022; Rossi et al., 2016) distributions. We follow Rossi et al., (2016) and use a two-parameter Weibull distribution described by a shape parameter (c_x) that describes daily variability and a scale (x_0) parameter related to the mean of the distribution, where:

$$pdf(x; x_0, c_x) = \frac{c_x}{x_0}\left(\frac{x}{x_0}\right)^{c_x-1} exp^{-1(x/x_0)^{cx}} \quad (3)$$

This distribution is used to characterize both daily precipitation (p_0, c_p) and daily runoff (r_0, c_r). Interpretations of fit parameters primarily focus on the shape parameter because it describes the right tail of daily values. We will colloquially refer to the shape parameter as the variability. Larger values of c_x indicate lower variability (i.e., smaller relative differences between daily runoff values), where c_x=1 is equivalent to the exponential distribution.

To estimate shape parameters, we follow Wilson & Toumi (2005) and perform a linear fit on the natural log linearized right tail of the exceedance frequency distribution above a threshold. On the transformed data, the shape parameter, c_x, is the slope of the regression, and the scale parameter, x_0, is exp(-intercept/slope) of the regression. Because parametric fits will be sensitive to threshold choice, distribution parameters were calculated using two thresholds for the daily runoff data, the upper 5% and upper 1% of daily values. Figures and discussion are based on the 1% threshold for both runoff and precipitation distributions. While threshold choice did alter the best-fit values for c_r, suggesting that a simple Weibull distribution is not able to fully characterize all cases, this variation in c_r did not substantially alter the relative spatial patterns in runoff variability. Runoff parameters were calculated on both the daily streamflow data (HCDN-2009) and the daily total runoff data from WaterGAP3. Pixel-based values in WaterGAP3 are not directly comparable to the watershed-averaged ones in HCDN-2009. In the following section, we address this challenge in the context of validating water model runoff data against observations.

4.2. Runoff Parameter Validation

Prior validation of WaterGAP3 data suggests that model data robustly reproduce mean river discharge from gauging stations (Beck et al., 2017; Eisner, 2015; Schmied et al., 2014, 2020). None of these prior assessments considered how well daily runoff variability is represented. Given the importance of daily runoff variability to bedrock river incision modeling, it is thus important to assess the extent to which shape parameters calculated from WaterGAP3 are consistent with those observed at stream gauges. For the sake of comparison, we first screened the HCDN-2009 network using the same topographic criteria used to screen WaterGAP3. Namely, we excluded watersheds where catchment relief (i.e., maximum minus minimum elevation within the catchment) is less than 500 meters and where mean elevation is less than 250 meters. Of the retained sites, we also imposed the additional criterion that HCDN-2009 daily runoff records are >95% complete within the WaterGAP3 time period (January 1,

1980 - December 31, 1999). We also removed data that occurs on leap days because these days are not calculated in the WaterGAP3 time series.

Once candidate HCDN-2009 stations were identified for validation, we needed to process the WaterGAP3 data to enable fair comparison. The first approach uses the mean runoff and runoff variability parameters calculated for each pixel in WaterGAP3. By oversampling these raster datasets of stochastic parameters to 1.5 seconds per pixel, HCDN-2009 watershed boundaries were used to calculate spatially averaged values of runoff parameters. While this treatment may be valid for small HCDN-2009 watersheds of similar scale to the WaterGAP3 pixels, this calculation may be problematic for larger watersheds where runoff should be routed downstream. As such, the second approach uses watershed boundaries to clip and route the WaterGAP3 data for each day within the 20-year time series. The mean runoff and shape parameter of the routed data are then calculated for the daily, routed data at the river outlet. For this computationally intensive approach, we used TopoToolbox (Schwanghart & Scherler, 2014) to: (1) acquire SRTM-90 digital elevation models (DEMs) for each watershed via the OpenTopography API, (2) project each DEM to the Universal Transverse Mercator (UTM) projection, (3) clip each day of the WaterGAP3 data to the watershed boundary and resample to the resolution of the DEM, (4) route discharge through the basin to build a time series of daily runoff at the outlet of each watershed, and (5) calculate mean runoff and shape parameters for the outlet time series.

4.3. Global Analysis

After understanding the strengths and limitations of WaterGAP3, this model data was used to identify the strongest predictors of mean runoff and daily runoff variability globally. The global analysis used two complementary approaches: (1) Develop relationships between mean runoff and variability (e.g., Molnar et al., 2006; Rossi et al., 2016), in a way that can account for the potential influence of snowmelt, and (2) Use unsupervised machine learning to probe the WaterGAP3 data and help identify strong predictors of mean runoff, snowmelt, and runoff variability.

For the first approach, we used the snowmelt fraction (Eq. 1) to partition the filtered WaterGAP3 data (see Section 3.1) into bins. Within each bin, we fit both a linear and a power law function relating mean runoff and the shape parameters of each pixel within that bin. This approach was motivated by empirical (Rossi et al., 2016) and ecohydrological modeling (Deal et al., 2018) studies that show how climatically driven gradients in daily runoff variability differ between rainfall-runoff and snowmelt-runoff regimes. For example, Rossi et al. (2016) showed that watersheds with lower snowmelt contributions were better described by a power law relationship between mean runoff and its associated Weibull shape parameter. In contrast, regions with higher snowmelt contributions showed a more linear relationship between these parameters. To compare the fits of both functions, we consider both the RMSE and the reduced chi-squared statistic under the view that that minimization of RMSE and/or reducing the chi-squared statistic closer to one should indicate the ‘better’ fit to the data.

In the second approach, we consider a larger suite of hydro-climatological, topographic, and geographic variables. Random forest regression (RFR) was used to assess the relative importance of potential predictor variables with respect to a given ‘target’ variable (Grömping, 2009). Target variables are hydro-climatic ones chosen based on their potential relevance to relationship between mean runoff and runoff variability (i.e., mean temperature, mean

precipitation, mean runoff, daily runoff variability, and snowmelt fraction). The list of predictor variables are broader and varied according to each target. Predictor variables included topographic (mean elevation, maximum elevation, mean local relief), geographic (latitude), and hydro-climatic (mean temperature, mean precipitation, daily precipitation variability, mean runoff, daily runoff variability, and snowmelt fraction) variables. We also attempted to thin predictor variables and remove what amounts to duplicates, e.g., as described in the results, latitude is the primary predictor of mean annual temperature and thus for other RFRs, we only include MAT as opposed to both MAT and latitude. Ultimately, we are not interested in the prediction per se, but to use the RFR to help identify which variables emerge as the most viable candidates linking mean runoff, snowmelt fraction, and daily runoff variability. In particular, we sought to discover which and whether any of the topographic metrics can be used to generalize hydro-climatic relationships that may co-evolve with growing topography.

4.4. Regional Cases

As we discuss in the context of our findings below, the global analysis revealed that generalizable relationships between topography and hydro-climatology were difficult to isolate at this largest spatial scale. While the global analysis reinforced the notion that snowmelt fraction mediates the relationship between mean runoff and daily runoff variability, scatter in these relationships clearly reflect the geographic diversity of montane hydrology. Furthermore, the lack of unambiguous topographic predictors that could be used to build rules for co-evolving stochastic parameters with the growth of mountain ranges limits the utility of the results from the global analysis to the application of 1D bedrock river incision modeling (Forte & Rossi, In Review). As such, we identified relationships between topography and stochastic runoff specific to individual mountain ranges, where differences in regional climate and geography can be partially accounted. To do this regional analysis, we used a 2° rectangular moving window to calculate the Spearman's rank correlation coefficient between candidate topographic variables and hydro-climatological ones. The topographic variables considered were the same as in the global analysis (mean elevation, maximum elevation, and mean local relief). The hydroclimatic variables we focused on were mean runoff and snowmelt fraction, the latter of which can be linked to daily runoff variability using relationships from the global analysis. We opt to focus on snowmelt fraction instead of daily runoff variability directly because the hypothesis we are trying to test in the 1D river incision modeling (Forte & Rossi, In Review) is how and whether snowmelt dynamics alter interpretations of stream power based analyses of river profiles. The results of the rank correlation analysis were used as the basis of selecting three regions where well-defined relationships can be developed between topography and hydro-climate. Specifically, these regional cases focus on the mid-latitude mountains of British Columbia, European Alps, and the Greater Caucasus (Figure 2), where snowmelt contributes a sizable fraction of daily streamflow.

5 Results

5.1 Validation of WaterGAP3

Figure 3 summarizes the results from our validation of WaterGAP3 model data against historical observations from select HCDN-2009 stream gages. The mean values for both datasets plot around the 1:1 line without obvious bias (Figure 3A), lending support to prior assessments (e.g., Beck et al., 2017; Eisner, 2015; Schmied et al., 2014, 2020). However, scatter around this

relationship shows that a >25% mismatch in mean values is not unusual. In general, simple spatial averaging performs almost as well as the computationally intensive routed approach, though routing matters for individual cases. For lower values of the shape parameter (i.e., higher runoff variability), the correspondence between the observations and the water model is relatively good (Figure 3B). At higher shape parameters (i.e., lower daily runoff variability) though, WaterGAP3 values are systematically lower than the HCDN-2009 gage data. This implies that WaterGAP3 tends to *overestimate* variability for these watersheds. For these lower variability watersheds, the routed version of WaterGAP3 does improve water model performance (Figure 3B), but does not remove the systematic bias. The residuals of the mismatch between the HCDN-2009 and WaterGAP3 values do not reveal a relationship between the mean and variability (Figure 3C), which might occur if the WaterGAP3 model was systematically altering storage-release relationships in hydrographs (e.g., due to limitations in how hydrologic processes are represented in the model). However, comparison of the residuals of the shape parameter to the mean annual temperature each the watershed (Figure 3D) indicates one possible interpretation for why variability in lower variability watersheds is overestimated in the WaterGAP3 data. The majority of lower variability basins tend to occur in colder settings, suggesting the possibility that snowmelt processes are not being adequately represented in the WaterGAP3 data. The direction of the mismatch is consistent with the notion that snow storage and release may not be fully resolved in WaterGAP3 data even though mean runoff is well represented in the water model.

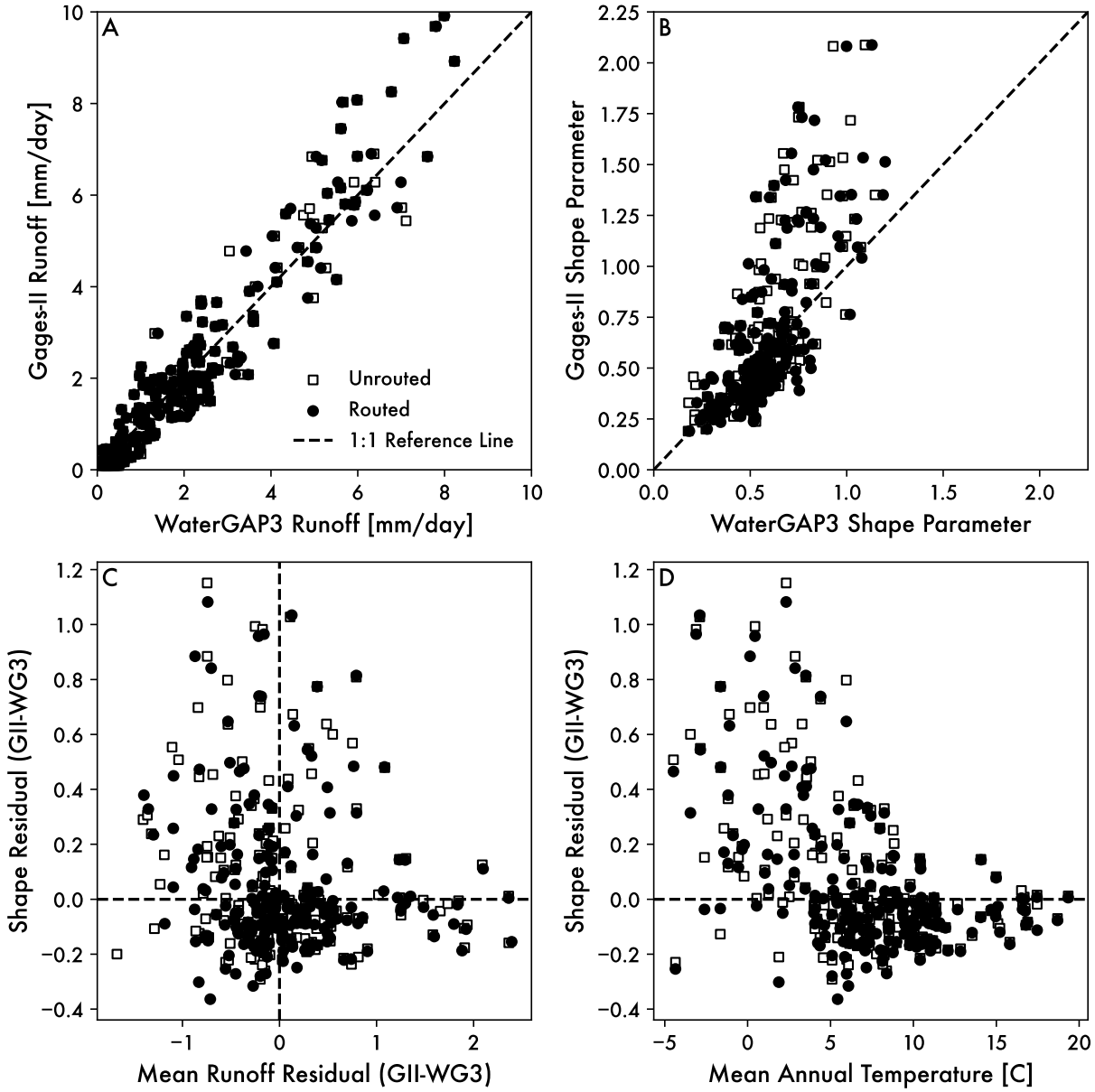

Figure 3. Comparison of WaterGap3 runoff parameters against selected HCDN-2009 stream gage data: (A) Mean runoff values, (B) Shape parameters of daily distributions, (C) Mean and shape residuals with respect to 1:1 line, and (D) Shape residuals against mean annual temperatures for each watershed. Open squares are arithmetic means of WaterGAP3 values within watershed boundaries. Closed circles route daily WaterGAP3 data to generate a time series that is then used to calculate fit parameters. Dashed lines in all panels indicate the 1:1 relationship between the water model and gaged data.

While systematic differences between model and empirical estimates of daily runoff variability is an important limitation to consider, we continue to use WaterGAP3 as our base dataset for a few reasons: (1) It is globally uniform, allowing for comparison of stochastic runoff in diverse settings, and (2) The systematic bias in variability has been quantified so that its

effects can be considered. Importantly, the bias in WaterGAP3 estimates of daily runoff variability lead to a *conservative* estimate of the dynamics we are examining in our 1D modeling of bedrock river incision (Forte & Rossi, In Review). Because hypothesized orographic feedbacks induce lower runoff variability as a mountain range grows, thereby increasing the degree of nonlinearity between channel steepness and erosion rate, it is preferable for the underlying rules setting these feedbacks to overestimate variability than the alternative.

5.2 Global relationships (relating mean and variability)

Figures 4-5 summarize the results for how mean runoff and runoff variability are related after binning the data by snowmelt fraction. Across all bins, WaterGAP3 data show that mean runoff is inversely related to daily runoff variability, consistent with prior studies (e.g., Molnar et al., 2006; Rossi et al., 2016). The large gridded WaterGAP3 dataset allowed us to more systematically explore these relationships at relatively fine (5%) intervals of snowmelt fraction (Figure 4). Each subpanel in Figure 4 is a heatmap showing the density of WaterGAP3 pixels for a given pair of best-fit parameters of the mean and shape of the distribution. Regressions on the pixel-level data are shown (solid lines show the better fit between linear and power law regressions). HCDN-2009 observational data are also shown as points for reference. Figure 4 demonstrate that it would be difficult to constrain these relationships using observational data alone because representation of different snowmelt fractions can be sparse, especially at higher snowmelt fractions. More importantly, it shows that the functional form of the relationship between the mean and variability changes from sublinear to linear with increasing snowmelt fraction. Using Figure 4 as our guide, we identified a snowmelt fraction of 0.35 as the transition where sublinear relationships give way to linear relationships between mean runoff and the shape parameter of the daily runoff distribution. Note that this transition is higher than the 10% threshold used to delineate snowmelt from rainfall-runoff dominated watersheds in Rossi et al. (2016). This disparity likely arises from two factors. First, that prior analysis focused on the snow fraction of precipitation and not the snowmelt fraction of runoff. Second, the sparsity of observations at higher snowmelt fractions in the HCDN-2009 data is not sufficient to define such a threshold.

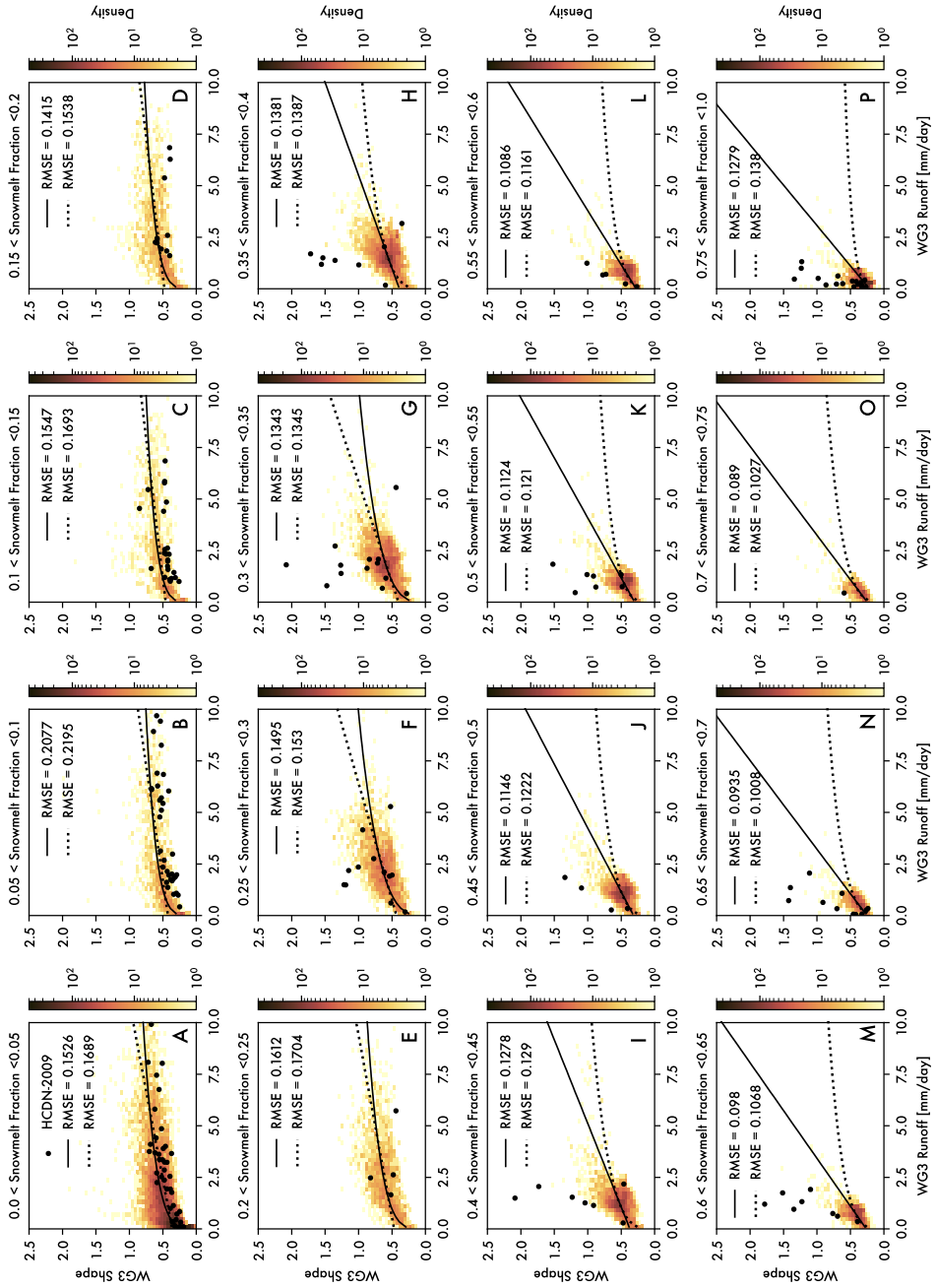

Figure 4. Density plots show the relationship between the shape parameter and mean runoff for the filtered WaterGAP3 data: (A-O) Plots binned by snowmelt fraction in increments of 0.05 up to 0.75 snowmelt. (P) The last panel is for the remaining data that has >0.75 snowmelt. In all panels, both a power law and linear fit are shown. The better fit is shown using a solid line and is based on having a lower RMSE. Results are the same if using the reduced chi squared statistic. Black dots are HCDN-2009 watersheds filtered in the same way. For HCDN-2009 data, snowmelt fraction was taken from WaterGAP3 data.

To more succinctly summarize these findings, Figure 5 shows the same plots by binning the data above and below a threshold snowmelt fraction of 0.35. The best of the regression lines

from Figure 4 are also plotted for reference. Figure 5 shows that individual regressions largely cluster around each other, especially in the domain where they are well constrained by data. It also shows that the relative spread of parameter values is smaller when there is a high fraction of snowmelt. The linear relationships shown at higher snowmelt fractions (Figure 5B) are strongly underestimating the value of the shape parameter as estimated from gaged basins, consistent with validation results (Figure 3B). Nevertheless, empirical observations still suggest a linear relationship between mean runoff and daily runoff variability at these higher snowmelt fractions. At lower snowmelt fractions, the observational data lie on the lower end of the envelopeWaterGAP3 pixels, which is demonstrated by the fact that regression lines predict slightly larger values of the shape parameter (Figure 5A). Again though, the functional form of these data is highly sublinear, much like shown in previous studies (Molnar et al., 2006; Rossi et al., 2016). Taken as a whole, these results suggest that the transition from rainfall dominated to snowmelt influenced parameters for stochastic runoff is relatively abrupt. Furthermore, our estimates of this transition using WaterGAP3 data provide conservative estimates of orographic feedbacks on runoff variability where both the mean and snowmelt fraction are expected to increase as mountain topography grows. It is conservative because biases in the water model data tend to dampen contrasts between rainfall and snowmelt dominated hydrology, and thus our 1D bedrock river incision modeling uses rulesets with weaker feedbacks than might be expected in reality (Forte & Rossi, In Review).

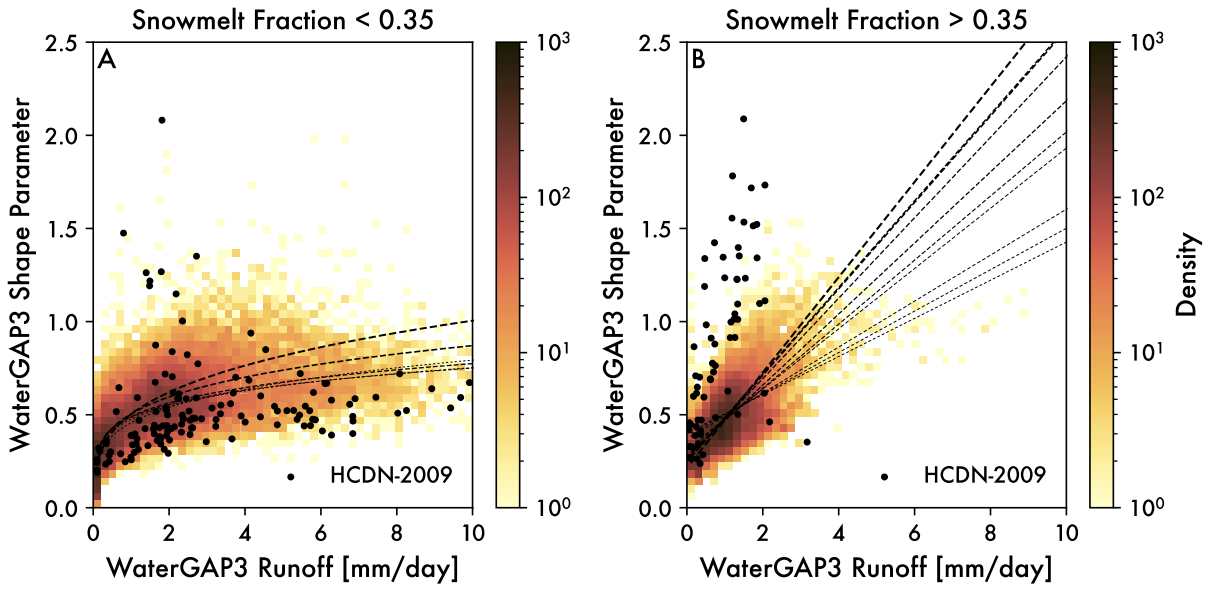

Figure 5. Density plots show the relationship between the shape parameter and mean runoff for the filtered WaterGAP3 data in the same way as Figure 4, only binning the data above and below a snowmelt fraction of 0.35: (A) Relationship for rainfall-dominated runoff, and (B) Relationship for snowmelt-influenced runoff parameters. Black dots are HCDN-2009 watersheds filtered in the same way. The strongest regressions from Figure 4 subpanels (solid lines) are shown for reference.

While analyzing the global water model data was motivated by prior studies that identified an inverse relationship between mean runoff and daily runoff variability in the

contiguous U.S. (Molnar et al., 2006; Rossi et al., 2016), we felt it also important analyze the global data more generically and suss out whether hydro-climatic parameters can be linked to topography itself. This latter objective is essential to building orographic rules that relate stochastic runoff parameters to mountain range growth and decay. To this end, we opted to use Random Forest Regression to partition the relative influence of topographic, geographic, and hydro-climatic predictors on a smaller subset of target variables.

5.3 Global relationships (Random Forest Regression)

Figure 6 summarizes the results of the random forest regression (RFR) analysis performed on global, filtered WaterGAP3 data. While principally interested in understanding the controls on mean runoff (Figure 6E-F), daily runoff variability (Figure 6G-H), and snowmelt fraction (Figure 6I-J), we also consider influences on other hydro-climatological variables that emerged as important determinants of these target variables, specifically mean annual temperature (Figure 6A-B) and mean precipitation (Figure 6C-D). The results of the RFR are not particularly surprising, but do shed some light on potential causal chains that links mean runoff, snowmelt fraction, and daily runoff variability as a mountain range grows.

Mean annual temperature and mean precipitation are the two strongest predictors of both mean runoff and snowmelt fraction, with temperature exerting a stronger influence on snowmelt fraction and precipitation exerting a stronger influence on runoff. Mean runoff itself is the strongest predictor of the shape of the daily runoff distribution, which supports our initial casting of this problem as building relationships between mean runoff and daily runoff variability (e.g., Figures 4,5). Other predictors of the shape of the runoff distribution are more evenly spread across the other hydro-climatic variables (i.e., daily precipitation shape, mean precipitation, snowmelt fraction, mean temperature in order of rank). That the shape of daily precipitation is partially encoded in the daily runoff distribution supporting similar findings when comparing rainfall regimes in the mid-latitudes to tropical sites (Rossi et al., 2016). That mean temperature and precipitation exhibit a knock-on effect in addition to their strong control on mean runoff emphasizes the importance of these two variables. Importantly, topographic metrics were weak predictors of all three principal targets (mean runoff, snowmelt fraction, daily runoff variability). This may be due to the fact that topography is expected to exert its influence via precipitation and temperature. To assess this, we also set mean precipitation and temperature as target variables in the RFR. The relative predictive power of three topographic metrics and mean temperature on mean precipitation is relatively uniform. In contrast, latitude is the strongest predictor of mean temperature with mean elevation providing modest predictive power. At this scale of analysis, topography does not appear to emerge as a strong predictor in the RFR modeling.

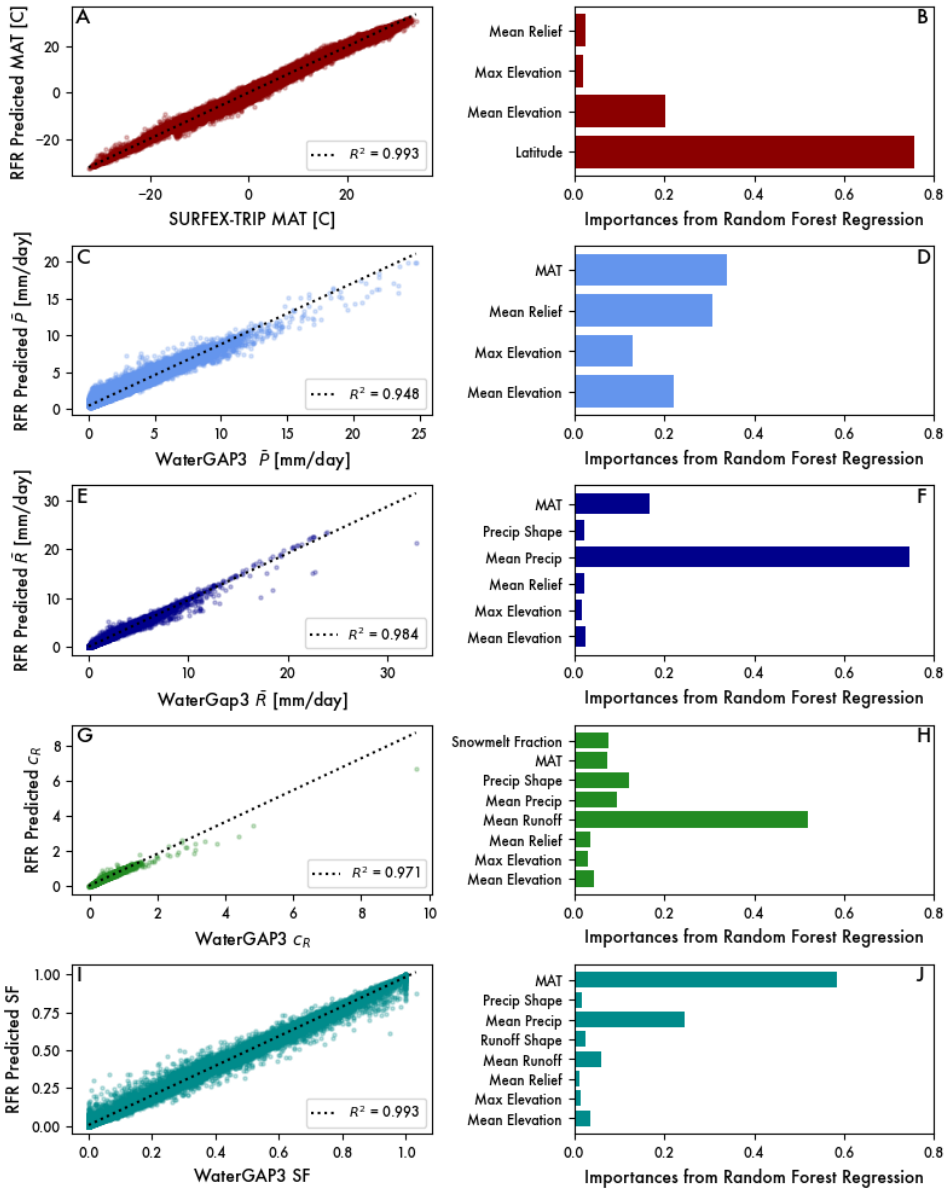

Figure 6. Results from the random forest regression for predicting: (A-B) Mean Temperature, (C-D) Mean Precipitation, (E-F) Mean Runoff, (G-H) Runoff Variability, and (I-J) Snowmelt Fraction. For each target variable, the left plot compares observed versus predicted data (linear fit with R^2 shown for reference), and the right plot shows the relative importance of predictors.

To further probe how topographic relationships might be obscured in this global analysis, we binned the pixel-level data by its mean temperature and precipitation, which emerged above as first-order controls on snowmelt fraction and mean runoff. We first removed outlier values using the method described by Doane (1976) where bin boundaries are defined after clipping variables to values below the 99.9th percentile. Membership in a given bin was determined by the mean temperature and precipitation of the pixel in question. Within each temperature-precipitation bin, we calculated Spearman's rank correlation coefficient between one of three topographic metrics (mean elevation, maximum elevation, and mean local relief) and either mean

runoff or snowmelt fraction. A correlation coefficient is only calculated if there are at least 10 pixels within a given temperature-precipitation bin and if the significance of the correlation coefficient exceeds the 95% confidence interval. We used Spearman's rank correlation coefficient because it does not assume linear correlation.

Figure 7 summarizes the results of the correlation analysis of WaterGAP3 data after binning by mean temperature and precipitation. The colors in plots show correlations between topography and mean runoff (top row) and correlations between topography and snowmelt fraction (bottom row). Green values indicate strong positive correlations, magenta values indicate strong negative correlations, black values indicate weak to no correlation, and grey values indicate that there was not enough observations in the dataset to evaluate correlation. The patterns in correlation are somewhat difficult to interpret as clusters of strong positive correlation are often adjacent to clusters of strong anti-correlation. Topographic predictors of mean runoff show little sensible pattern (Figures 7A-C), with a hint of positive correlation between local relief and mean runoff at low values of mean precipitation (Figures 7C). Topographic predictors of snowmelt fraction are also complex with a band of positive correlation for lower mean temperatures next to a band of anti-correlation at higher temperatures (Figures 7D-F). While we hesitate to interpret these subtle patterns, the snowmelt fraction results do suggest that increasing topographic elevation and relief only leads to more snowmelt where temperatures are conducive to it, though why this relation has a slope is not obvious.

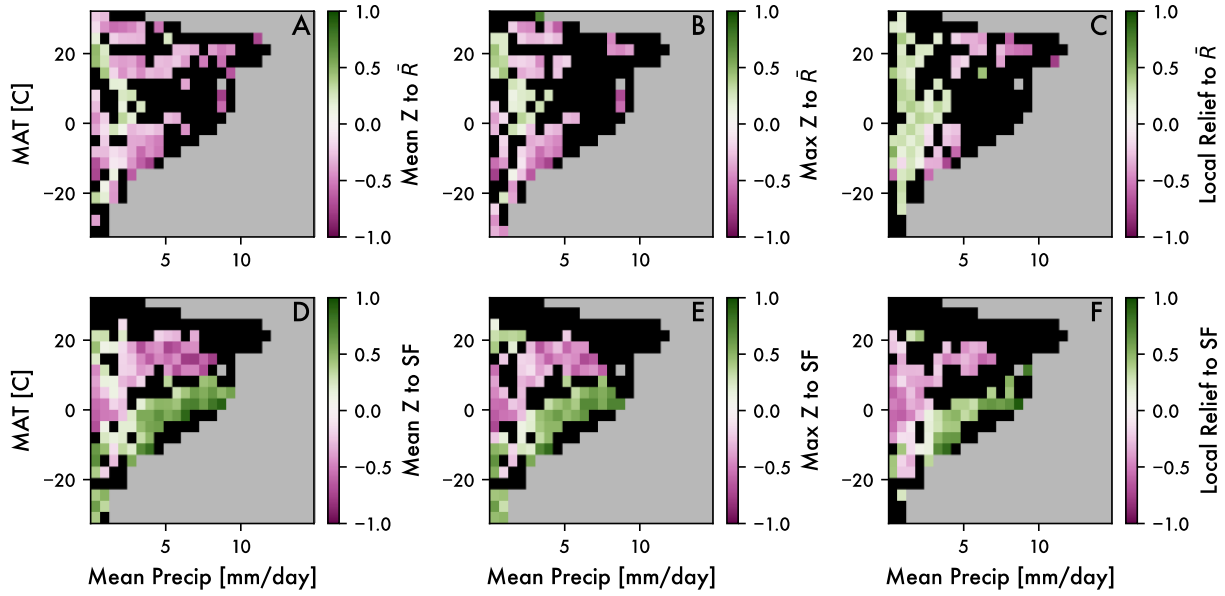

Figure 7. Spearman's rank correlation coefficients within temperature-precipitation bins. (A-C) Coefficients relating topography and mean runoff. (D-F) Coefficients relating topography to snowmelt fraction. The topographic variables considered were mean elevation (A, D), maximum elevation (B, E), and local relief (C, F). For all plots, the gray area indicates regions of parameter space with less than 10 observations. Black regions indicate there were greater than 10 observations, but that the correlation did not exceed the 95% confidence interval.

As we discuss in more depth in the discussion below, the results from the global analysis suggest that there is no single set of globally applicable 'rules' that relate topography to mean

runoff and snowmelt fraction. We suspect this is a consequence of the scale of the analysis (i.e., orographic effects are inherently regional) and the lack of accounting for the predominant direction of weather systems with respect to topography (i.e., steep topography is not distinguished as windward versus leeward). Based on this, we next explore a set of three regional analyses that show more promise in constraining orographic controls on mean runoff and snowmelt fraction.

5.4 Regional relationships of mean runoff and daily runoff variability

Given the challenge of identifying simple relationships between topography (i.e., mean elevation, maximum elevation, and mean local relief) and either mean runoff or snowmelt fraction (Figures 6-7), we now examine whether regional relationships between these variables are being obscured by the global treatment. Of the six relationships shown in Figure 7, the relationship between local relief and mean runoff and the relationship between maximum elevation and snowmelt fraction seemed the most promising when evaluated spatially. Figure 8 summarizes the sign and strength of these relationships for all WaterGAP3 data that meet our selection criteria. The zoom insets highlight three regions of interest – namely the mid-latitude mountains of British Columbia, European Alps, and the Greater Caucasus. Each of these mountain ranges receive a large fraction of their precipitation as snow, with some alpine glaciation under modern climate. In these settings (and others), there is a relatively strong correlation between local relief and mean runoff across the study area (Figure 8A-insets), consistent with prior studies (Bookhagen & Burbank, 2006; Bookhagen & Strecker, 2008). The relationship between maximum elevation and snowmelt fraction is more nuanced (Figure 8B-insets). The sign of the correlation depends on the whether positioned on the windward or leeward side of prevailing weather systems, whereby windward sides show relatively strong positive correlations. Nevertheless, the most complex of these three regional sites is the Greater Caucasus, where relationships among maximum elevation, snowmelt fraction, and runoff generation has been verified using a finer-scale analysis of gauge records and hydroclimatic data (Forte et al., 2022). Taken as whole, this gives us confidence that these three locations are prime candidates for building regional relationships among topography, snowmelt, and runoff statistics.

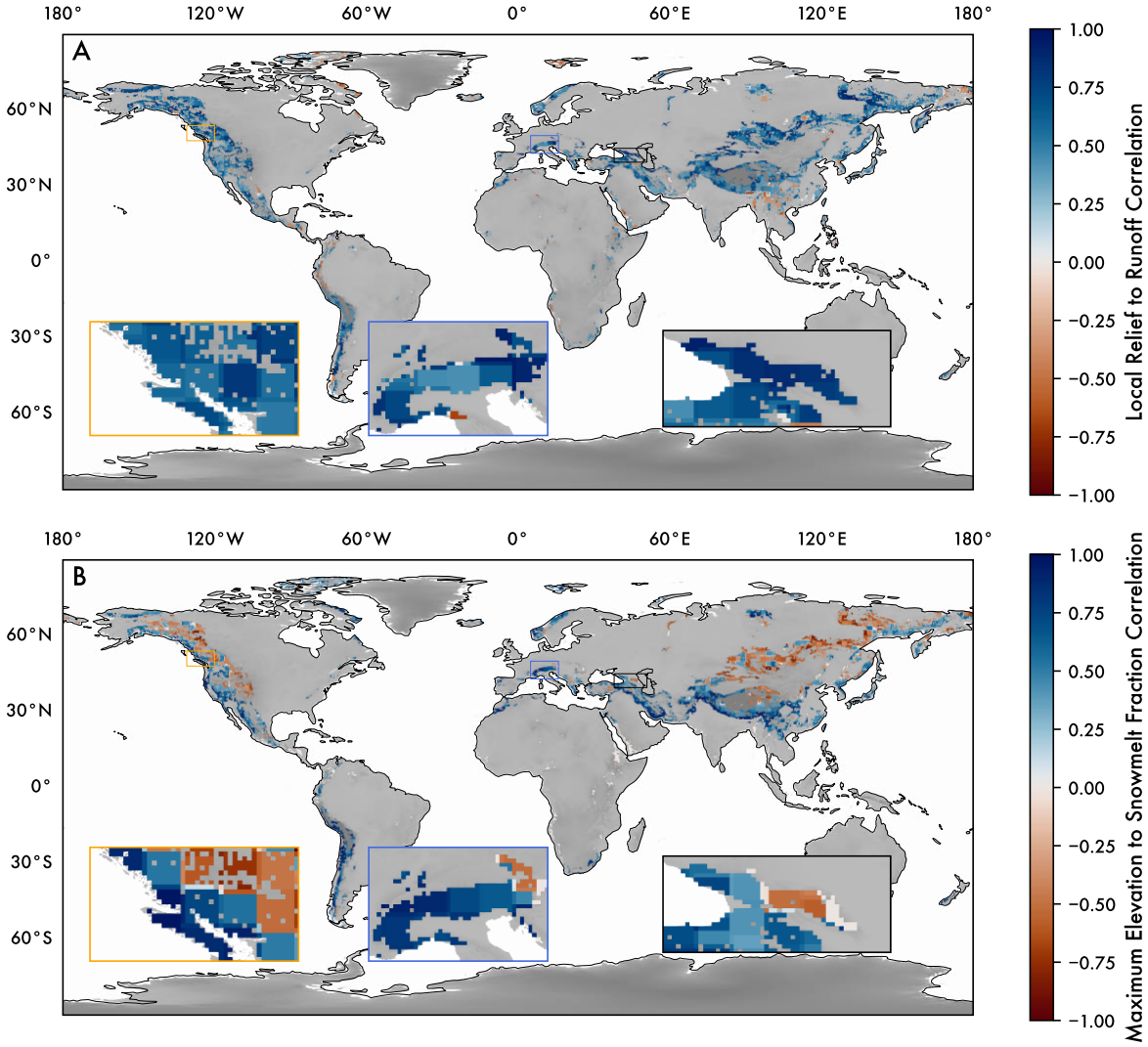

Figure 8. Relationships among topography, mean runoff, and snowmelt fraction in map view. (A) Mean spearman rank correlation coefficient within a 2° moving window for mean runoff and local relief. (B) Mean spearman rank correlation coefficient within a 2° moving window for maximum elevation and snowmelt fraction. After filtering the WaterGAP3 data for mountain settings (see text for details), only a small area remains. Insets highlight results for the three regional cases considered.

6 Discussion

6.1 Mean runoff, runoff variability, and snowmelt

The global analysis of WaterGAP3 data helped solidify interpretations that mean runoff and daily runoff variability are inversely correlated. This result was born out both in the Random Forest Regression (Figure 6) and in the individual regressions after binning by snowmelt fraction (Figures 4-5), thereby supporting findings from prior studies based on stream gauge data (Molnar et al., 2006; Rossi et al., 2016). The functional form of the relationship between mean runoff and the shape of the daily runoff distribution appears to bifurcate at snowmelt fractions around 0.35

(Figure 5). Below this value, the relationship is highly nonlinear and suggestive of dynamics based on ecohydrological modeling (Deal et al., 2018). Above this value, relationships vary but become much more linear. The transition to snowmelt hydrology resulting in lower variability flows (e.g., Pitlick, 1994) is expected due to the effects of both increased runoff ratios and the slow release of water from storage. That this transition is abrupt emphasizes the importance of the phase transition from rain to snow in event-scale runoff variability. The snowmelt fractions where this occurs are relatively low suggesting that snowmelt should not be ignored in fluvial erosion models. We also note here that stochastic-threshold models based on stream power were originally developed for small watersheds (e.g., Lague et al., 2005; Tucker, 2004). Given our focus on mountain range scales, it is important to also understand how the spatial footprint of runoff events varies for different runoff generation mechanisms.

To assess the importance of spatial scale to runoff generation, Figure 9 compares the exceedance frequency of the spatial footprints of precipitation and runoff events in the WaterGAP3 data. The area of each 'event' is determined by finding spatially contiguous objects in the daily data above a given intensity threshold (i.e., 5 - 35 mm/day). To convert the unprojected pixel-based objects into areas, we multiplied the number of pixels by the size of a pixel in degrees squared. We then calculated the radius of the circle that equals that area. The radius of the circle is converted from degrees to km in both latitude and longitude. Because the conversion in longitude generally differs from the conversion in latitude, this transformation produces an ellipse with area units of km^2. These are the x-coordinates used for plotting exceedance frequencies (Figure 9A,C,E,G). Furthermore, for runoff data, we labeled each event as snowmelt or rainfall runoff based on the 0.35 snowmelt fraction threshold. Because smaller footprints include both rainfall and snowmelt dominated runoff, the right hand panels (Figure 9B,D,F,H) shows the percent of daily runoff events that are classified as snowmelt for log distributed bins of exceedance frequency. Three important insights emerge from this analysis. First, and unsurprisingly, higher intensity thresholds produce smaller event areas. Second, at around the 25 mm/day threshold, the largest area events in runoff and precipitation (i.e., far right tails) are of similar magnitude. Higher thresholds produce runoff areas larger than comparable frequency precipitation events. Third, the far right tail of the size distribution of runoff is all snowmelt. Taken together, these results suggest that the relative contribution of snowmelt runoff becomes increasingly important for larger watersheds and for increasing intensities.

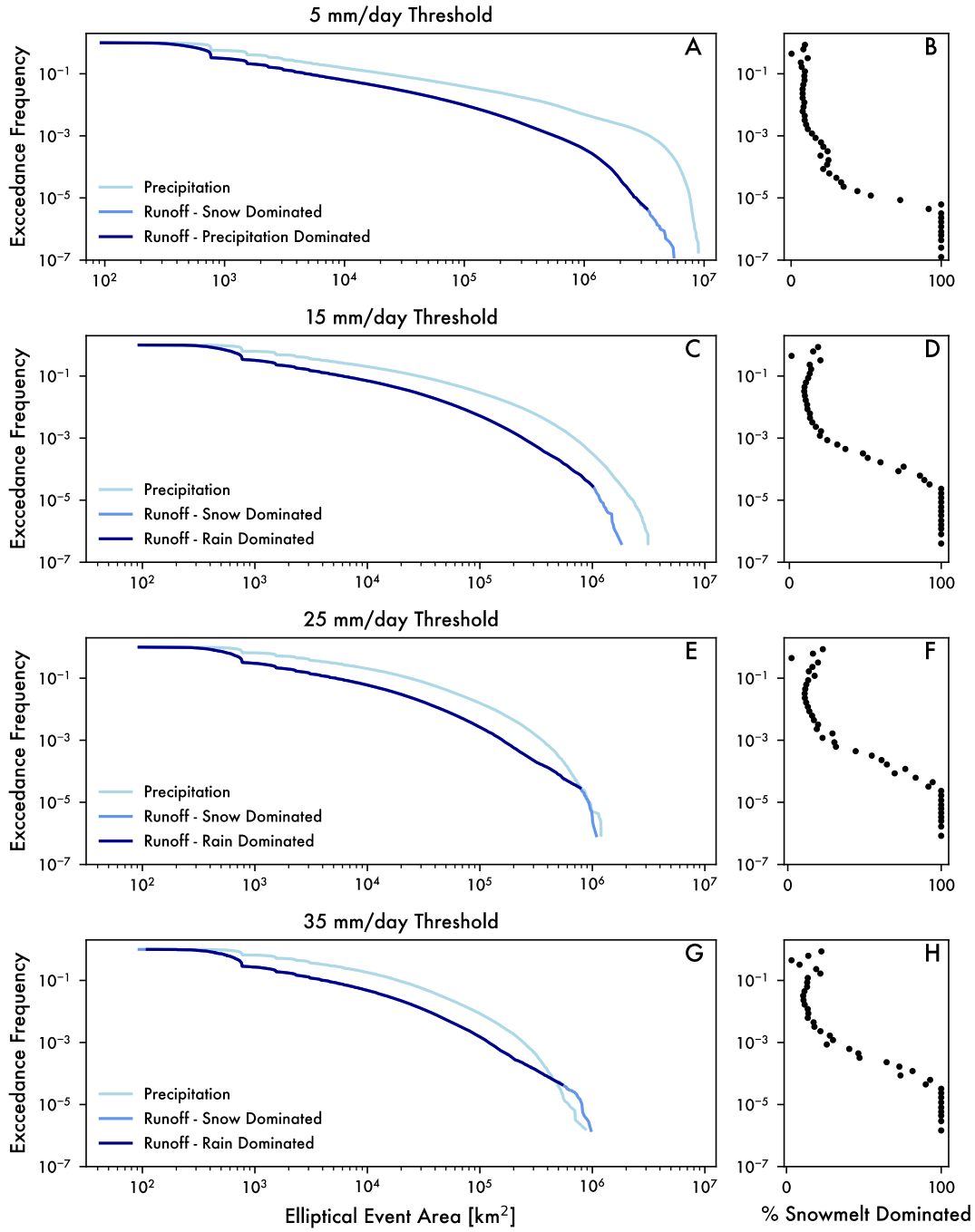

Figure 9. Exceedance probability distributions of daily event sizes of different magnitudes: (A-B) 5 mm/day, (C-D) 15 mm/day, (E-F) 25 mm/day, and (G-H) 35 mm/day. The left panels show probability plots for both precipitation and runoff, whereby the latter is color-coded by runoff generation source. After classifying runoff events in this way, the right panels show what fraction of events are snowmelt dominated within exceedance probability bins. Note that regardless of intensity threshold the largest area runoff events are snowmelt dominated. At higher intensity thresholds, these event sizes can exceed the largest area precipitation events.

6.2 Importance of constraining regional relationships

While global relationships linking mean runoff and daily runoff variability via topography were elusive, regional assessment was much more promising. Figure 10 summarizes the kinds of regional rulesets that can be generated from an analysis like ours. The pixel-based correlation coefficients presented earlier (Figure 8) are summarized into bins of either mean runoff or snowmelt fraction (y-axes). For each bin, the mean and standard deviation of the correlated topographic metric is shown (local relief for mean runoff and maximum elevation for snowmelt fraction). Marker sizes are scaled to the number of observations within a bin. Power law fits for each relationship are shown as lines. Each region is described by its own functional relationship, which we interpret as the orographic effects on mean runoff and snowmelt fraction for each mountain range. We suspect that some of the non-monotonic behavior of binned values, especially in snowmelt fraction, are a consequence of mixing windward and leeward components of a regional orographic effect (e.g., Figure 8), as well as along-strike complexity in precipitation sourcing. Nevertheless, summarizing the data in this way allows us to build empirically based rules for mean runoff and snowmelt fraction specific to each region. Together with the observation that the relationship between mean runoff and daily runoff variability abruptly shifts around snowmelt fractions of 0.35 allows us to drive a stochastic runoff model using regionally informed parameters from WaterGAP3 in part 2 of this analysis (Forte & Rossi, In Review).

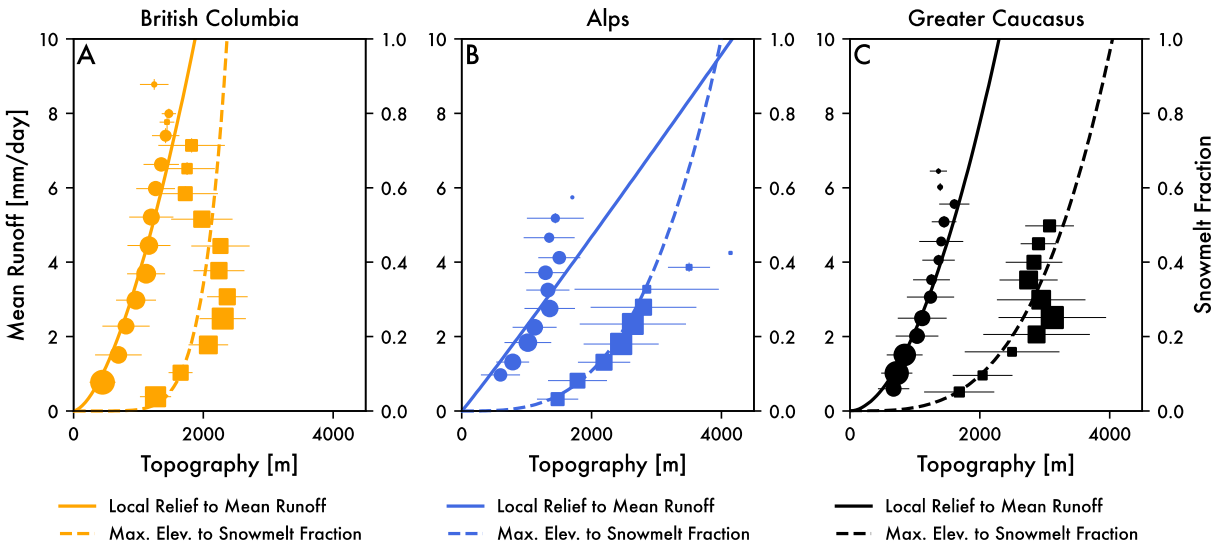

Figure 10. Relationships among topography, mean runoff, and snowmelt fraction for the three regional cases (see Figure 8 for locations): (A) British Columbia, (B) European Alps, and (C) Greater Caucasus. In all three plots, circles are binned mean runoff to local relief, and squares are binned snowmelt fraction to maximum elevation. Symbols are scaled to number of observations in the bin and whiskers show one standard deviation. Power law fits for binned data relate local relief and mean runoff (solid line) and maximum elevation and snowmelt fraction

(dashed line). These fits serve as the basis for orographic rules used in our complementary model study (Forte & Rossi, In Review).

The relationships shown in Figure 10 help explain why the role of topography was so hard to extract from the Random Forest Regression (RFR) that included these metrics (Figure 6). First, regional relationships relating topography to runoff generation are quite noisy. While casting runoff parameters as a simple function of topography was our goal, the relatively coarse resolution of water model data, the lack of distinguishing between windward from leeward slopes, and hydro-climatic diversity induced by regional climate will each confound simple relationships between topography and runoff parameters. Second, while the power law functions decently describe snowmelt fraction, the bin-averaged values suggest subtle, non-monotonic relationships with maximum elevation. Third, and perhaps most importantly, the relationship for each regional setting are distinctly different. Any global analysis would struggle to parse this difference.

6.3 Implications on landscape evolution studies

Two-way coupled models between climate and tectonics require erosion laws for either river incision, glacial erosion, or both. Those testing fluvial dynamics are typically built on the stream power model (e.g., Beaumont et al., 1992; Stolar et al., 2006; Whipple & Meade, 2004; Willett, 1999). Orographic effects in these models focus on the windward ascent and extraction of precipitation. By setting up a contrast in the efficiency of erosion on the windward and leeward sides of mountain ranges, mountain belts adjust their width and height in order to achieve a steady state morphology. The widespread use of stream power in these climate-tectonic models has subsequently motivated many studies to interrogate how orographically induced spatial patterns in precipitation might alter the long-term evolution of river profiles and relief (Anders et al., 2008; Han et al., 2014; Leonard & Whipple, 2021; Roe et al., 2002, 2003). At the same time, stream power models are increasingly incorporating the role of stochastic streamflow and erosion thresholds to interpret river profiles (DiBiase & Whipple, 2011; Lague, 2014; Lague et al., 2005; Marder & Gallen, 2023; Snyder et al., 2003; Tucker, 2004; Tucker & Bras, 2000). As such, the aim in this study was integrate these two productive research threads and explore whether mean runoff, daily runoff variability, and snowmelt fraction can be linked to each other via topographic elevation and relief.

Figure 11 is a conceptual cartoon illustrating how stochastic runoff parameters might co-evolve with mountain topography in settings where mountain range relief is sufficient to trigger the transition from rainfall-dominated to snowmelt-influence runoff, but where river incision is still setting the relief structure of the landscape (e.g., Whipple et al., 1999). The color coded dots on the schematic mountains in Figure 11A are intended to correspond to the dots on the hypothetical plots relating topography to runoff and snowmelt (Figure 11B) and those relating mean runoff to daily runoff variability (Figure 11C). On the windward side of mountain ranges we expect that the growth of topography will increase mean runoff (Figure 11B solid line) in line with conventional treatments of orographic precipitation (Roe, 2005). This leads to concurrent increases in the frequency of snowfall and thus the snowmelt contribution to runoff (Figure 11B dashed line). While snowmelt fraction has an upper bound of one, in practice, the upper bound we are envisioning in Figure 11B will be less than one because rain continues to fall at lower elevations and because the temperatures required to enhance very high snowmelt fractions would also entail a transition to glaciation. The key behavior in this conceptual framework is that

accounting for snowmelt dynamics leads to a markedly different relationship between mean runoff and the shape parameter of the daily runoff distribution (Figure 11C). Our global analysis of WaterGAP3 data suggests that this transition might be abrupt, with snowmelt fractions of 0.35 marking a dramatic decrease in daily runoff variability (Figures 4-5). The strength and form of these relationships need to be assessed independently for any given mountain range (Figure 10). However, by simplifying the hydrology into just two parameters, these kinds of relationships are well-suited to driving long term models of river incision (e.g., Lague et al., 2005; Tucker, 2004) in ways that can be linked to mean climate (DiBiase & Whipple, 2011) and ecohydrology (Deal et al., 2018).

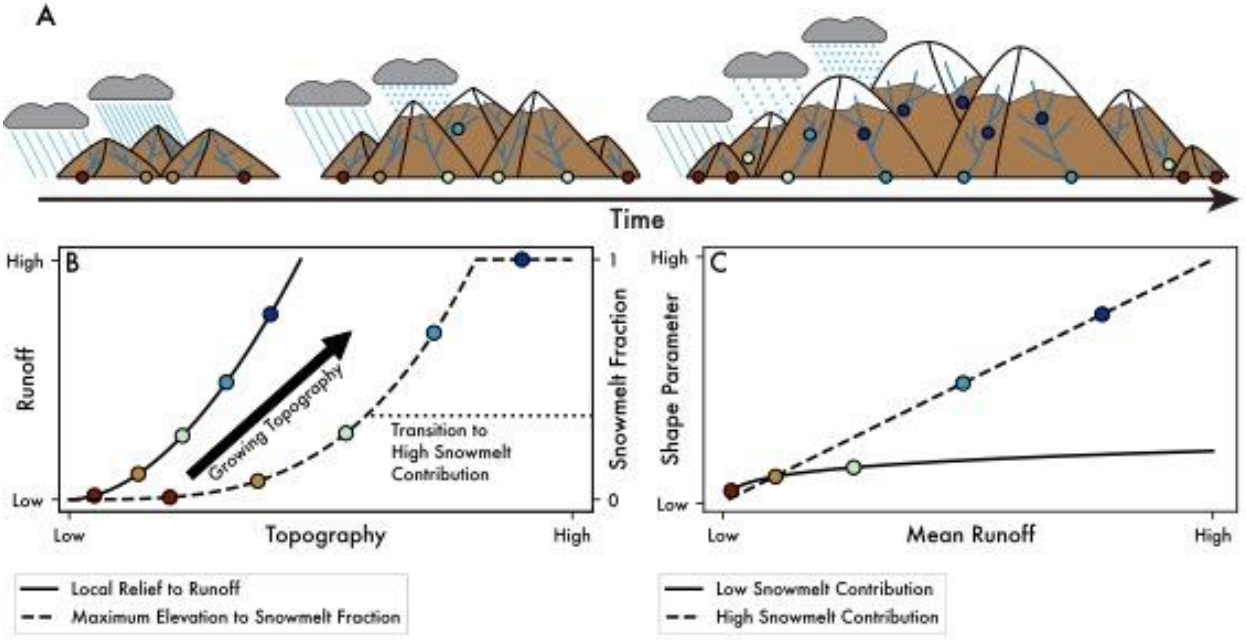

Figure 11. Conceptual model for how orographic controls on runoff variability can be represented in a landscape evolution model. (A) Cartoon showing how precipitation and runoff generation mechanisms might change as a mountain range grows. (B) Example rules for how topography is translated into more runoff and a larger snowmelt fraction as topography grows. (C) Relationship between mean runoff and daily runoff variability in response to those rules. In B, the example ruleset shows that as mountain topography grows, increasing relief leads to more runoff generation on the windward side of a mountain range and increasing elevations lead to a higher fraction of snowmelt. In C, these topography-runoff relationships translate into a much different relationship between mean runoff and daily runoff variability that encodes the transition from rainfall- to snowmelt-dominated runoff events.

While we think there is observational evidence for these dynamics in actual landscapes (Forte et al., 2022), we highlight a few important caveats to generalizing from our large-scale analysis of the WaterGAP3 water model data. First, this conceptual model is better suited to explaining the windward side of mountain ranges where precipitation, and thus runoff, is enhanced by topography. To build better rulesets, higher resolution runoff datasets that honor physiographic transitions and water divides are likely needed. Second, this conceptual model requires that mean runoff and extreme runoff events are linked via some common mechanism. This need not be the case. For example, recent work in the Colorado Front Range showed how

mean runoff was largely driven by snowmelt throughout the landscape while daily runoff variability was driven by rainfall runoff at lower elevations in response to thinning soils (Rossi et al., 2020). Such mechanistic controls on mean runoff and daily runoff variability are at play in all landscapes and may partially explain the wide variance of runoff parameters observed in our regional rulesets (Figure 10). Third, statistical analyses all assumed independence of daily runoff events which is decidedly not true as runoff events, especially large ones, can extend over multiple days (synoptic-scale storms) to seasons (snowmelt, monsoons). Despite these caveats, this analysis produced empirically-based runoff parameters that vary in space and time. As such, this provides the minimal constraints needed to integrate orographic effects with stochastic runoff generation for river profile modeling (Forte & Rossi, In Review).

7. Conclusions

The results of our global analysis of WaterGAP3 data largely confirm, and significantly expand upon, past results indicating a negative correlation between mean runoff and daily runoff variability. The form of the relationship between variability and mean runoff is linked to the fraction of runoff from snowmelt. For snowmelt fractions <0.35, mean runoff and variability are related via a power law. At higher snowmelt fractions, the two are linearly related. We also find that snowmelt produces runoff events with a much larger areal extent than rainfall runoff.

Exploration of the extent to which mean runoff, runoff variability, and snowmelt fraction are related to topography produces ambiguous results at the global scale. Unsupervised machine learning methods highlight that simple topographic variables such as mean elevation, maximum elevation, and local relief do not have strong predictive power for our target hydroclimatological parameters of mean runoff, snowmelt fraction, and daily runoff variability. Attempts to identify cross-correlations that may be masking the role of topography were more suggestive, but still difficult to interpret. Results from the global analysis emphasize that exploring relationships between topography and hydroclimatology requires a regional approach. For three mid-latitude mountain ranges - the European Alps, Greater Caucasus, and southern British Columbia – we find robust positive relationships between mean runoff and mean local relief and snowmelt fraction and maximum elevation.

The links between topography, mean runoff, daily runoff variability, and snowmelt fraction highlight that multiple aspects of hydroclimate of mountain ranges should be expected to evolve as topography grows. Past work on this topic has primarily focused on the influence of growing topography on the development of orographic patterns in rainfall. When coupled to tectonic models and simple hydrologic models equating patterns in mean rainfall to mean runoff, orographic effects have been shown to drive a variety of feedbacks between surface processes and tectonics. Our results show how to move beyond mean precipitation or mean runoff when considering the coupled evolution of topography, tectonics, and climate. Both snowmelt fraction and mean runoff are expected to increase with growing topography and reduce daily runoff variability, emphasizing the need to explicitly consider snowmelt dynamics in coupled tectonic – landscape evolution models.

Acknowledgments

Support for M.W. Rossi came from the Geomorphology and Land-use Dynamics (GLD) Program (EAR-1822062). Neither AMF or MWR have any real or perceived financial or other conflicts with the contents of this work.

Open Research

Analysis codes necessary to reproduce this work are housed in the GitHub repository (https://github.com/amforte/snowmelt_orography) with stable release doi: 10.5281/zenodo.8115140. Larger outputs of the processing steps are available through the Zenodo repository doi:10.5281/zenodo.7665887. Portions of these analysis codes rely on publicly available datasets that we do not have permission to redistribute, but when used, we provide comments in the code referencing where these datasets can be downloaded.

References

Adam, J. C., Hamlet, A. F., & Lettenmaier, D. P. (2009). Implications of global climate change for snowmelt hydrology in the twenty-first century. *Hydrological Processes*, *23*(7), 962–972. https://doi.org/10.1002/hyp.7201

Adams, B. A., Whipple, K. X., Forte, A. M., Heimsath, A. M., & Hodges, K. V. (2020). Climate controls on erosion in tectonically active landscapes. *Science Advances*, *6*(42). https://doi.org/10.1126/sciadv.aaz3166

Alcamo, J., Döll, P., Henrichs, T., Kaspar, F., Lehner, B., Rösch, T., & Siebert, S. (2003). Development and testing of the WaterGAP 2 global model of water use and availability. *Hydrological Sciences Journal*, *48*(3), 317–337. https://doi.org/10.1623/hysj.48.3.317.45290

Anders, A. M., Roe, G. H., Montgomery, D. R., & Hallet, B. (2008). Influence of precipitation phase on the form of mountain ranges. *Geology*, *36*(6), 479. https://doi.org/10.1130/G24821A.1

Barnett, T. P., Adam, J. C., & Lettenmaier, D. P. (2005). Potential impacts of a warming climate on water availability in snow-dominated regions. *Nature*, *438*(7066), 303–309. https://doi.org/10.1038/nature04141

Barnhart, T. B., Molotch, N. P., Livneh, B., Harpold, A. A., Knowles, J. F., & Schneider, D. (2016). Snowmelt rate dictates streamflow. *Geophysical Research Letters*, *43*(15), 8006–8016. https://doi.org/10.1002/2016GL069690

Barros, A. P., & Lettenmaier, D. P. (1994). Dynamic modeling of orographically induced precipitation. *Reviews of Geophysics*, *32*(3), 265. https://doi.org/10.1029/94RG00625

867 Basso, S., Merz, R., Tarasova, L., & Miniussi, A. (2023). Extreme flooding controlled by stream network
868 organization and flow regime. *Nature Geoscience*, *16*(4), 339–343. https://doi.org/10.1038/s41561-023-
869 01155-w
870 Beaumont, C., Fullsack, P., & Hamilton, J. (1992). Erosional control of active compressional orogens. In K. R.
871 McClay (Ed.), *Thrust Tectonics* (pp. 1–18). New York: Chapman Hall.
872 Beck, H. E., van Dijk, A. I. J. M., de Roo, A., Dutra, E., Fink, G., Orth, R., & Schellekens, J. (2017). Global
873 evaluation of runoff from 10 state-of-the-art hydrological models. *Hydrology and Earth System Sciences*,
874 *21*(6), 2881–2903. https://doi.org/10.5194/hess-21-2881-2017
875 Berghuijs, W. R., Woods, R. A., & Hrachowitz, M. (2014). A precipitation shift from snow towards rain leads to a
876 decrease in streamflow. *Nature Climate Change*, *4*(7), 583–586. https://doi.org/10.1038/nclimate2246
877 Berghuijs, W. R., Harrigan, S., Molnar, P., Slater, L. J., & Kirchner, J. W. (2019). The Relative Importance of
878 Different Flood-Generating Mechanisms Across Europe. *Water Resources Research*, *55*(6), 4582–4593.
879 https://doi.org/10.1029/2019WR024841
880 Bookhagen, B., & Burbank, D. (2006). Topography, relief, and TRMM-derived rainfall variations along the
881 Himalaya. *Geophysical Research Letters*, *33*, L08405–L08405. https://doi.org/10.1029/2006GL026037
882 Bookhagen, B., & Burbank, D. (2010). Toward a complete Himalayan hydrological budget: Spatiotemporal
883 distribution of snowmelt and rainfall and their impact on river discharge. *Journal of Geophysical Research*,
884 *115*(F03019). https://doi.org/10.01029/02009JF001426
885 Bookhagen, B., & Strecker, M. R. (2008). Orographic barriers, high-resolution TRMM rainfall, and relief variations
886 in the eastern Andes. *Geophysical Research Letters*, *35*(L06403). https://doi.org/10.1029/2007GL032011
887 Bookhagen, B., & Strecker, M. R. (2011). Modern Andean Rainfall Variation during ENSO Cycles and its Impact
888 on the Amazon Drainage Basin. In C. Hoorn & F. P. Wesselingh (Eds.), *Amazonia: Landscape and Species*
889 *Evolution* (pp. 223–241). Oxford, UK: Wiley-Blackwell Publishing Ltd.
890 https://doi.org/10.1002/9781444306408.ch14
891 Botter, G., Porporato, A., Rodriguez-Iturbe, I., & Rinaldo, A. (2009). Nonlinear storage-discharge relations and
892 catchment streamflow regimes: STREAMFLOW REGIMES OF NONLINEAR CATCHMENT. *Water*
893 *Resources Research*, *45*(10). https://doi.org/10.1029/2008WR007658

894 Campforts, B., Vanacker, V., Herman, F., Vanmaercke, M., Schwanghart, W., Tenorio, G. E., et al. (2020).
895 Parameterization of river incision models requires accounting for environmental heterogeneity: insights
896 from the tropical Andes. *Earth Surface Dynamics*, *8*(2), 447–470. https://doi.org/10.5194/esurf-8-447-2020
897 Crave, A., & Davy, P. (2001). A stochastic "precipiton" model for simulating erosion/sedimentation dynamics.
898 *Computers & Geosciences*, *27*(7), 815–827. https://doi.org/10.1016/S0098-3004(00)00167-9
899 Deal, E., Favre, A. C., & Braun, J. (2017). Rainfall variability in the Himalayan orogen and its relevance to erosion
900 processes. *Water Resources Research*, *53*(5), 4004–4021. https://doi.org/10.1002/2016WR020030
901 Deal, E., Braun, J., & Botter, G. (2018). Understanding the Role of Rainfall and Hydrology in Determining Fluvial
902 Erosion Efficiency. *Journal of Geophysical Research: Earth Surface*, *123*(4), 744–778.
903 https://doi.org/10.1002/2017JF004393
904 Decharme, B., Alkama, R., Douville, H., Becker, M., & Cazenave, A. (2010). Global Evaluation of the ISBA-TRIP
905 Continental Hydrological System. Part II: Uncertainties in River Routing Simulation Related to Flow
906 Velocity and Groundwater Storage. *Journal of Hydrometeorology*, *11*(3), 601–617.
907 https://doi.org/10.1175/2010JHM1212.1
908 Decharme, B., Martin, E., & Faroux, S. (2013). Reconciling soil thermal and hydrological lower boundary
909 conditions in land surface models: LOWER BOUNDARY CONDITIONS OF SOIL IN LSM. *Journal of*
910 *Geophysical Research: Atmospheres*, *118*(14), 7819–7834. https://doi.org/10.1002/jgrd.50631
911 Desormeaux, C., Godard, V., Lague, D., Duclaux, G., Fleury, J., Benedetti, L., et al. (2022). Investigation of
912 stochastic-threshold incision models across a climatic and morphological gradient. *Earth Surface*
913 *Dynamics*, *10*(3), 473–492. https://doi.org/10.5194/esurf-10-473-2022
914 DiBiase, R. A., & Whipple, K. X. (2011). The influence of erosion thresholds and runoff variability on the
915 relationships among topography, climate, and erosion rate. *Journal of Geophysical Research*, *116*(F04036).
916 https://doi.org/10.1029/2011JF002095
917 DiBiase, R. A., Whipple, K. X., Heimsath, A. M., & Ouimet, W. B. (2010). Landscape form and millennial erosion
918 rates in the San Gabriel Mountains, CA. *Earth and Planetary Science Letters*, *289*(1–2), 134–144.
919 Doane, D. P. (1976). Aesthetic Frequency Classifications. *The American Statistician*, *30*(4). Retrieved from
920 https://amstat.tandfonline.com/doi/abs/10.1080/00031305.1976.10479172

Döll, P., Kaspar, F., & Lehner, B. (2003). A global hydrological model for deriving water availability indicators: model tuning and validation. *Journal of Hydrology*, *270*(1–2), 105–134. https://doi.org/10.1016/S0022-1694(02)00283-4

Eagleson, P. S. (1978). Climate, soil, and vegetation: 2. The distribution of annual precipitation derived from observed storm sequences. *Water Resources Research*, *14*(5), 713–721. https://doi.org/10.1029/WR014i005p00713

Eisner, S. (2015). *Comprehensive evaluation of the waterGAP3 model across climatic, physiographic, and anthropogenic gradients*. University of Kassel.

Falcone, J. A. (2011). *GAGES-II: Geospatial Attributes of Gages for Evaluating Streamflow* (Report). Reston, VA. https://doi.org/10.3133/70046617

Farr, T. G., Rosen, P. A., Caro, E., Crippen, R., Duren, R., Hensley, S., et al. (2007). The shuttle radar topography mission. *Reviews of Geophysics*, *45*, 1–33.

Fatichi, S., Vivoni, E. R., Ogden, F. L., Ivanov, V. Y., Mirus, B., Gochis, D., et al. (2016). An overview of current applications, challenges, and future trends in distributed process-based models in hydrology. *Journal of Hydrology*, *537*, 45–60. https://doi.org/10.1016/j.jhydrol.2016.03.026

Forte, A. M., & Rossi, M. W. (In Review). Stochastic in Space and Time: Part 2, Effects of Simulating Orographic Gradients in Daily Runoff Variability on Bedrock River Incision. *Journal of Geophysical Research - Earth Surface*.

Forte, A. M., Whipple, K. X., Bookhagen, B., & Rossi, M. W. (2016). Decoupling of modern shortening rates, climate, and topography in the Caucasus. *Earth and Planetary Science Letters*, *449*, 282–294. https://doi.org/10.1016/j.epsl.2016.06.013

Forte, A. M., Leonard, J. S., Rossi, M. W., Whipple, K. X., Heimsath, A. M., Sukhishvili, L., et al. (2022). Low variability runoff inhibits coupling of climate, tectonics, and topography in the Greater Caucasus. *Earth and Planetary Science Letters*, *584*. https://doi.org/10.1016/j.epsl.2022.117525

Galewsky, J. (2009). Rain shadow development during the growth of mountain ranges: An atmospheric dynamics perspective. *Journal of Geophysical Research*, *114*(F1), F01018. https://doi.org/10.1029/2008JF001085

Grömping, U. (2009). Variable Importance Assessment in Regression: Linear Regression versus Random Forest. *The American Statistician*, *63*(4), 308–319. https://doi.org/10.1198/tast.2009.08199

949 Han, J., Gasparini, N. M., Johnson, J. P. L., & Murphy, B. P. (2014). Modeling the influence of rainfall gradients on
950 discharge, bedrock erodibility, and river profile evolution, with application to the Big Island, Hawai'i.
951 *Journal of Geophysical Research*, *119*, 1418–1440. https://doi.org/10.1002/203JF002961
952 Harel, M. A., Mudd, S. M., & Attal, M. (2016). Global analysis of the stream power law parameters based on
953 worldwide 10Be denudation rates. *Geomorphology*, *268*, 184–196.
954 https://doi.org/10.1016/j.geomorph.2016.05.035
955 Howard, A. D. (1994). A detachment-limited model of drainage basin evolution. *Water Resources Research*, *30*(7),
956 2261–2285.
957 Huang, X., & Niemann, J. D. (2006). An evaluation of the geomorphically effective event for fluvial processes over
958 long periods: GEOMORPHICALLY EFFECTIVE EVENT. *Journal of Geophysical Research: Earth*
959 *Surface*, *111*(F3), n/a-n/a. https://doi.org/10.1029/2006JF000477
960 Jiang, Q. (2003). Moist dynamics and orographic precipitation. *Tellus A: Dynamic Meteorology and Oceanography*,
961 *55*(4), 301. https://doi.org/10.3402/tellusa.v55i4.14577
962 Kirby, E., & Whipple, K. X. (2012). Expression of active tectonics in erosional landscapes. *Journal of Structural*
963 *Geology*, *44*, 54–75.
964 Kirchner, J. W. (2009). Catchments as simple dynamical systems: Catchment characterization, rainfall-runoff
965 modeling, and doing hydrology backward: CATCHMENTS AS SIMPLE DYNAMICAL SYSTEMS.
966 *Water Resources Research*, *45*(2). https://doi.org/10.1029/2008WR006912
967 Lague, D. (2014). The stream power river incision model: evidence, theory and beyond. *Earth Surface Processes*
968 *and Landforms*, *39*(1), 38–61. https://doi.org/10.1002/esp.3462
969 Lague, D., Hovius, N., & Davy, P. (2005). Discharge, discharge variability, and the bedrock channel profile. *Journal*
970 *of Geophysical Research*, *110*, F04006–F04006. https://doi.org/10.1029/2004JF000259
971 Laherrère, J., & Sornette, D. (1998). Stretched exponential distributions in nature and economy: "fat tails" with
972 characteristic scales. *The European Physical Journal B*, *2*(4), 525–539.
973 https://doi.org/10.1007/s100510050276
974 Lehner, B., Verdin, K., & Jarvis, A. (2008). New Global Hydrography Derived From Spaceborne Elevation Data.
975 *Eos, Transactions American Geophysical Union*, *89*(10), 93. https://doi.org/10.1029/2008EO100001

976 Leonard, J. S., & Whipple, K. X. (2021). Influence of Spatial Rainfall Gradients on River Longitudinal Profiles and
977 the Topographic Expression of Spatially and Temporally Variable Climates in Mountain Landscapes.
978 *Journal of Geophysical Research: Earth Surface*, *126*(12). https://doi.org/10.1029/2021JF006183
979 Leonard, J. S., Whipple, K. X., & Heimsath, A. M. (2023). Isolating climatic, tectonic, and lithologic controls on
980 mountain landscape evolution. *Science Advances*, *9*(3), eadd8915. https://doi.org/10.1126/sciadv.add8915
981 Lins, H. F. (2012). *USGS hydro-climatic data network 2009 (HCDN-2009)* (US Geological Survey Fact Sheet 3047
982 No. 4). Retrieved from https://pubs.usgs.gov/fs/2012/3047/pdf/fs2012-3047.pdf
983 Malamud, B. D., & Turcotte, D. L. (2006). The applicability of power-law frequency statistics to floods. *Journal of*
984 *Hydrology*, *322*(1–4), 168–180. https://doi.org/10.1016/j.jhydrol.2005.02.032
985 Marder, E., & Gallen, S. F. (2023). Climate control on the relationship between erosion rate and fluvial topography.
986 *Geology*. https://doi.org/10.1130/G50832.1
987 Molnar, P., Anderson, R. S., Kier, G., & Rose, J. (2006). Relationships among probability distributions of stream
988 discharges in floods, climate, bed load transport, and river incision. *Journal of Geophysical Research*, *111*,
989 F02001–F02001. https://doi.org/10.1029/2005JF000310
990 Nesbitt, S. W., & Anders, A. M. (2009). Very high resolution precipitation climatologies from the Tropical Rainfall
991 Measuring Mission precipitation radar: TRMM HIGH RESOLUTION PRECIPITATION. *Geophysical*
992 *Research Letters*, *36*(15), n/a-n/a. https://doi.org/10.1029/2009GL038026
993 Pitlick, J. (1994). Relation between peak flows, precipitation, and physiography for five mountain regions in the
994 western USA. *Journal of Hydrology*, *158*, 219–240.
995 Roe, G. H. (2005). OROGRAPHIC PRECIPITATION. *Annual Review of Earth and Planetary Sciences*, *33*(1), 645–
996 671. https://doi.org/10.1146/annurev.earth.33.092203.122541
997 Roe, G. H., Montgomery, D. R., & Hallet, B. (2002). Effects of orographic precipitation variations on the concavity
998 of steady-state river profiles. *Geology*, *30*(2), 143–146.
999 Roe, G. H., Montgomery, D. R., & Hallet, B. (2003). Orographic precipitation and the relief of mountain ranges.
1000 *Journal of Geophysical Research*, *108*(B6). https://doi.org/10.1029/2001JB001521
1001 Rossi, M. W., Whipple, K. X., & Vivoni, E. R. (2016). Precipitation and evapotranspiration controls on event-scale
1002 runoff variability in the contiguous United States and Puerto Rico. *Journal of Geophysical Research*, *121*.
1003 https://doi.org/10.1002/2015JF003446

1004 Rossi, M. W., Anderson, R. S., Anderson, S. P., & Tucker, G. E. (2020). Orographic Controls on Subdaily Rainfall
1005 Statistics and Flood Frequency in the Colorado Front Range, USA. *Geophysical Research Letters*, *47*(4).
1006 https://doi.org/10.1029/2019GL085086
1007 Schaefli, B., Rinaldo, A., & Botter, G. (2013). Analytic probability distributions for snow-dominated streamflow:
1008 Snow-Dominated Streamflow Pdfs. *Water Resources Research*, *49*(5), 2701–2713.
1009 https://doi.org/10.1002/wrcr.20234
1010 Schellekens, J., Dutra, E., Weiland, F. S., Minvielle, M., Calvet, J.-C., Decharme, B., et al. (2017). A global water
1011 resources ensemble of hydrological models: the eartH2Observe Tier-1 dataset.
1012 Scherler, D., DiBiase, R. A., Fisher, G. B., & Avouac, J.-P. (2017). Testing monsoonal controls on bedrock river
1013 incision in the Himalaya and Eastern Tibet with a stochastic-threshold stream power model. *Journal of*
1014 *Geophysical Research: Earth Surface*, *122*, 1389–1429. https://doi.org/10.1002/2016JF004011
1015 Schmied, H., Eisner, S., Franz, D., Wattenbach, M., Portmann, F. T., Flörke, M., & Döll, P. (2014). Sensitivity of
1016 simulated global-scale freshwater fluxes and storages to input data, hydrological model structure, human
1017 water use and calibration. *Hydrology and Earth System Sciences*, *18*(9), 3511–3538.
1018 https://doi.org/10.5194/hess-18-3511-2014
1019 Schmied, H., Cáceres, D., Eisner, S., Flörke, M., Herbert, C., Niemann, C., et al. (2020). The global water resources
1020 and use model WaterGAP v2.2d: Model description and evaluation. *Geoscientific Model Development*, *14*,
1021 1037–1079. https://doi.org/10.5194/gmd-2020-225
1022 Schwanghart, W., & Scherler, D. (2014). Short Communication: TopoToolbox 2 - MATLAB based software for
1023 topographic analysis and modeling in Earth surface sciences. *Earth Surface Dynamics*, *2*, 1–7.
1024 https://doi.org/10.5194/esurf-2-1-2014
1025 Shen, H., Lynch, B., Poulsen, C. J., & Yanites, B. J. (2021). A modeling framework (WRF-Landlab) for simulating
1026 orogen-scale climate-erosion coupling. *Computers & Geosciences*, *146*, 104625.
1027 https://doi.org/10.1016/j.cageo.2020.104625
1028 Shobe, C. M., Tucker, G. E., & Anderson, R. S. (2016). Hillslope-derived blocks retard river incision. *Geophysical*
1029 *Research Letters*, *43*(10), 5070–5078. https://doi.org/10.1002/2016GL069262

1030 Sivapalan, M., Jothityangkoon, C., & Menabde, M. (2002). Linearity and nonlinearity of basin response as a
1031 function of scale: Discussion of alternative definitions: TECHNICAL NOTE. *Water Resources Research*,
1032 *38*(2), 4-1-4–5. https://doi.org/10.1029/2001WR000482
1033 Smith, R. B. (1979). The Influence of Mountains on the Atmosphere. In B. Saltzman (Ed.), *Advances in Geophysics*
1034 (Vol. 21, pp. 87–230). Elsevier. https://doi.org/10.1016/S0065-2687(08)60262-9
1035 Smith, R. B., & Barstad, I. (2004). A Linear Theory of Orographic Precipitation. *Journal of the Atmospheric*
1036 *Sciences*, *61*(12), 1377–1391. https://doi.org/10.1175/1520-0469(2004)061<1377:ALTOOP>2.0.CO;2
1037 Snyder, N. P., Whipple, K. X., Tucker, G. E., & Merrits, D. J. (2003). Importance of a stochastic distribution of
1038 floods and erosion thresholds in the bedrock river incision problem. *Journal of Geophysical Research*,
1039 *108*(B2). https://doi.org/10.1029/2001JB001655
1040 Stolar, D. B., Willett, S. D., & Roe, G. H. (2006). Climatic and tectonic forcing of a critical orogen. In S. D. Willett,
1041 N. Hovius, M. T. Brandon, & D. Fisher (Eds.), *Tectonics, climate, and landscape evolution* (Vol. 398, pp.
1042 241–250). Geological Society of America.
1043 Trenberth, K. E., Dai, A., Rasmussen, R. M., & Parsons, D. B. (2003). The Changing Character of Precipitation.
1044 *Bulletin of the American Meteorological Society*, *84*(9), 1205–1218. https://doi.org/10.1175/BAMS-84-9-
1045 1205
1046 Tucker, G. E. (2004). Drainage basin sensitivity to tectonic and climatic forcing: Implications of a stochastic model
1047 for the role of entrainment and erosion thresholds. *Earth Surface Processes and Landforms*, *29*, 185–204.
1048 https://doi.org/10.1002/esp.1020
1049 Tucker, G. E., & Bras, R. L. (2000). A stochastic approach to modeling the role of rainfall variability in drainage
1050 basin evolution. *Water Resources Research*, *36*(7), 1953–1964.
1051 Walter, M. T., Brooks, E. S., McCool, D. K., King, L. G., Molnau, M., & Boll, J. (2005). Process-based snowmelt
1052 modeling: does it require more input data than temperature-index modeling? *Journal of Hydrology*, *300*(1–
1053 4), 65–75. https://doi.org/10.1016/j.jhydrol.2004.05.002
1054 Whipple, K. X. (2009). Landscape texture set to scale. *Nature*, *460*, 468–469.
1055 Whipple, K. X., & Meade, B. (2004). Controls on the strength of coupling among climate, erosion, and deformation
1056 in two-sided, frictional orogenic wedges at steady state. *Journal of Geophysical Research*, *109*, F01011–
1057 F01011. https://doi.org/10.1029/2003JF000019

1058 Whipple, K. X., & Tucker, G. E. (1999). Dynamics of the stream-power river incision model: Implications for
1059 height limits of mountain ranges, landscape response timescales, and research needs. *Journal of*
1060 *Geophysical Research*, *104*(B8), 17661–17674.
1061 Whipple, K. X., Kirby, E., & Brocklehurst, S. H. (1999). Geomorphic limits to climate-induced increases in
1062 topographic relief. *Nature*, *401*, 39–43.
1063 Whipple, K. X., Hancock, G. S., & Anderson, R. S. (2000). River incision into bedrock: Mechanics and relative
1064 efficacy of plucking, abrasion, and cavitation. *Geology*, *112*(3), 490–503.
1065 Whipple, K. X., DiBiase, R. A., Crosby, B., & Johnson, J. P. L. (2022). Bedrock Rivers. In J. (Jack) F. Shroder
1066 (Ed.), *Treatise on Geomorphology (Second Edition)* (pp. 865–903). Oxford: Academic Press.
1067 https://doi.org/10.1016/B978-0-12-818234-5.00101-2
1068 Willett, S. D. (1999). Orogeny and orography: The effects of erosion on the structure of mountain belts. *Journal of*
1069 *Geophysical Research*, *104*(B12), 28,957-28,981.
1070 Wilson, P. S., & Toumi, R. (2005). A fundamental probability distribution for heavy rainfall. *Geophysical Research*
1071 *Letters*, *32*(14). https://doi.org/10.1029/2005GL022465
1072 Wobus, C. W., Whipple, K. X., Kirby, E., Snyder, N. P., Johnson, J., Spyropolou, K., et al. (2006). Tectonics from
1073 topography: Procedures, promise, and pitfalls. In S. D. Willett, N. Hovius, M. T. Brandon, & D. Fisher
1074 (Eds.), *Tectonics, climate, and landscape evolution* (Vols. 1–398, pp. 55–74). Boulder, CO: The Geological
1075 Society of America.

1076